博士論文（要約）

Subject Specific Modeling of Bodies for Muscle Activity Estimation
Based on Geometric Morphing
（幾何学的モーフィングに基づいた筋活動推定のための
被験者固有身体モデリング）

池上　洋介

Subject Specific Modeling of Bodies for Muscle Activity Estimation Based on Geometric Morphing

A dissertation presented by

Yosuke Ikegami

The Department of Mechano-Informatics
Graduate School of Information Science and Technology

THE UNIVERSITY OF TOKYO

March 2017

Thesis advisor
Yoshihiko Nakamura

Author
Yosuke Ikegami

Subject Specific Modeling of Bodies for Muscle Activity Estimation Based on Geometric Morphing

Abstract

This dissertation studies the subject-specific modeling of bodies and the modeling of contacts with environment, which are required for the estimation of muscle forces from noninvasive measurement data on the basis of geometric characteristics for the individuals'.

In this dissertation, the useful important findings to model the subject-specific musculoskeletal systems are to be provided as follows: (1) The fundamental and simple-manner techniques of muscle modeling and inertial parameter modeling for large-DOF musculoskeletal systems on the basis of geometric characteristics of bodies are to be developed. Not only for the humans, but also through the modeling of heterogeneous mammals, especially for the mice, the wide range of applicability of developed techniques are to be perceived. (2) Through the development of the contact modeling, the method of practical motion analysis combined with multiple people are to be proposed. Especially, practical contact force estimation in multipoint become possible by solving the optimization problem for contact forces and muscle forces simultaneously considering force directions and somatosensory electromyography signals even if the contact forces can not be measured directly. (3) The quantitative assessment techniques for the large-DOF whole-body motor functions of the laboratory mice are to be newly developed ahead of the world through the presentation of the measurement techniques and the analysis results, which include the time-series data of the muscle tensions, joint torques, and joint trajectories.

The proposed methods and results to model the subject-specific musculoskeletal systems are to be appeared in the publication (in preparation).

Acknowledgments

This dissertation was written under the supervision of Professor Yoshihiko Nakamura. His constant support, encouragement, and stimulation were essential for the completion of this thesis. I would like to express my sincere gratitude to him.

And, five professors gave me exact comments to improve this thesis as reviewers: Professor Isao Shimoyama, Professor Ryohei Kanzaki, Professor Watatu Takano, Professor Masamichi Shimosaka, Dr Satoshi Oota, I especially thank Professor Wataru Takano and Dr Satoshi Oota for stimulating discussions about the research.

Special thanks to all ex- and current staffs of Nakamura laboratory. Professor Hiroshi Kaminaga, the assistant professor, Special thanks to Masamitsu Saitoh, Hirotaka Imagawa, Dr. Sreenivasa Manish, Dr. Akihiko Murai, gave me lots of technical advice in this work. Ms. Ayumi Maeda and Ms. Mika Ueno, the secretaries, helped me a lot on all office works. Especially I would like to thank Dr. Ko Ayusawa, frequently advised me from his considerable experience and always encouraged me.

Special thanks to all other ex- and current members of the lab in musculoskeletal systems, Yusuke Nakamura, Yuki Ibuka, Junichi Ishikawa, Taku Kashiwagi, Blasdel Aaron Michael, Dr. Sungsuk Ok, Kanade Kubota, Akihiro Yoshimatsu, Satochi Otsuki, Kensho Hirasawa, Kazunari Takeichi, Akio Hayakawa, Rohan Budhiraja, Yohan Shin, Elodie Millanvois, Thanh-Tin Phan Nguyen, Krithika Swaminathan, Emiko Uchiyama, Takuya Ohashi, Tatsuaki Machida, Ayaka Yamada, Jose Enrique Chen, Toshihiro Mino, Katsumasa Kitajima.

I would like to note that the part of This work was supported by Japan Society for the Promotion of Science under Category (S) of Grant-in-Aid for Scientific Research (20220001),“ Establishing Human-Machine Communication Through Kinesiology and Linguistics Integration ”(PI: Y. Nakamura). Finally, I thank my family and my greatest benefactor for their behind-the-scenes support in all non-technical issues.

Contents

List of Figures

List of Tables

Chapter1

Introduction

1.1 Goals of this dissertation

According to the theory of evolution by Charles Darwin in 1859, the process of evolution requires the following four conditions [13, 44]:

1. Living creatures lay children more than the number of those survive.
2. An individual in the same species has a variety of mutations.
3. Some mutations affect the probability of survival and reproductive capacity.
4. Some mutations that affect the probability of survival and reproduction capacity are inherited to children.

A mutation spreads in the population through the generations. It is the mechanism of evolution by natural selection. The genetic information of an individual is determined by the combination of the parents' genes and their mutations. The body and its functions, including the motor function, are formed as the gene phenotype. In the process of growth, an individual continues to change the body characteristics through development and acquisition under the influence of stress from the environments. Although the inheritance of an acquired character is controversial, it is safe to say that the character of an individual is formed by two factors, namely, the hereditary and environmental factors. The mutation appears in cells because of any a posteriori reasons. Only those that appear in the reproductive cells are inherited. Biological diversity indicates the large number of different species on earth and appears in large types of small differences in a species. The diversity is stored in the genetic system of

living species as the memory of evolution. The essence of the trait of living creatures is the genetic information transmitted through a long period [14].

The Wolff's law is a well-known theory in biomechanics, which was proposed in 1892 by the German orthopedist, Julius Wolff. The theory explains that the shape of a bone is formed by the applied force over a certain period. It also describes the rule of deformation. The bone shape is formed with a minimum weight that withstands the applied force. Therefore, the theory can be regarded as an optimization principle. Harold Frost proposed the Mechanostat Theory in 1960 as a refinement of the Wolff's law [40, 19, 20, 18, 21]. The theory explains that the reason of the bone shape change is not continuous, but dynamic stress. The applied peek force above the certain level induces the bone shape change. The increased bone density of the dominant hand of an athlete or the decreased bone density of an astronaut after a long stay in space or a person in bedridden life is considered the consequence of the Mechanostat Theory. The theory is supported by much data and now widely accepted. The shape and properties of the bone are originally planned and formed by the gene and continuously changed by the gravity force, muscle force, and applied forces from the environments. In other words, the Mechanostat Theory implies that the bone shape is formed by the interaction between the a priori phenotype of the gene and the a posteriori acquisition throughout life. Let us consider the Mechanostat Theory in a broader sense. It is the idea that biological shape is formed as a collective of its function. That is, functional information can be implicitly seen in the body shape information. The Mechanostat Theory and the Wolff's law explain that the bone is formed to make the bone functional under the load of life. Accordingly, we may say that the bone shape and properties characterize the environments, where the animal belongs. It would not be too ambitious to say that the bone shape and properties, including the bones and the muscles, characterize the life and functions of the animal.

This dissertation aims to typically explain the physical and functional properties of animals, human, and mammals at large by developing the modeling and analysis methods using the model. Even a simple movement of an animal is the result of the combined role of body motion elements, such as bones, muscles, tendons, and ligaments, of which activity signals are initiated at the central nerve system and transmitted through the connected neural system by neuro transmitters. The energy

of movement is supplied by the circulatory system and transferred via chemical reaction cycles. Many parameters are involved in this whole phenomenon, from macro parameters (e.g., bone weight and length) to micro parameters (e.g., the gap at a nerve junction and the distribution of mitochondria in the muscle fibers).

The scope of this dissertation lays in the subject-specific modeling of bodies. This is motivated by the thoughts that the information of life and functions is in the body shape and properties, and the difference of information is the essence of distinguishing the individuals. Note that the parametric modeling of the body shape and properties is considered to extract the essential parameters of life and functions. System modeling does not only mean the reconstruction of the exact physical phenomenon in a mathematical form, but also is the common and significant practice of modeling that would represent the best approximated behavior of the system using a small number of parameters in a sense of optimality. The Advanced Industrial Science and Technology Digital Human Center offers an open repository of the measured human body dimensions of a large Japanese population of different ages and areas of residency in Japan. The data set includes the data of approximately 500 persons and more than 250 kinds of body lengths belonging to each [35][29]. The principal component analysis of the data showed that only five principal components are sufficient to model the body geometry of the Japanese population with approximately 80% coverage.

Following the engineering technology development in recent years, robotics has rapidly developed in combination with information science and technology. The targeted degree of freedom (DOF) has increased its number. A large-DOF humanoid robot that mimics the human shape or a large-scale simulator has also been developed in the past few years. The simulator was created from the calculation method developed in the robotics fields and can calculate the joint trajectory, joint torque, and muscle tension in the motion. Furthermore, this simulator is actively used to analyze human motion and reflect the parameters determined from calculation to humanoid development design. In the field of sports science, an attempt to understand the features of the simulator was made by analyzing the movement of skilled athletes. Information about the shape of the model used in these simulators are a very important factor because it directly affects the analysis result. Trying to provide a practical subject-specific modeling for large-scale simulators is the second objective of

this dissertation. The social and technical background in problems with the motion analysis of the musculoskeletal simulator using the subject-specific model is presented in the next section away from shape and functionality.

1.2 Background

1.2.1 Subject specific musculoskeletal model

A musculoskeletal system model is necessary for the musculoskeletal motion analysis. The model should include the skeletal model for the kinematic analysis and the musculotendinous model for the motor function analysis. It is desirable to suppress the modeling error in the musculoskeletal model parameters intended for use by the simulator because it directly affects the analysis results.

The two types of models considered in this dissertation are the skeletal and muscle models. The skeletal model manages two types of parameters, namely the geometric parameter representing the joint distance and the marker position and dynamic parameter representing a mass center of gravity, inertia tensor. The generalized coordinates obtained from inverse kinematics is not the natural result if the geometric parameters are not correctly estimated. The error appears as a joint torque if the dynamic parameter is not correctly estimated. One of the parameter errors also becomes the cause of the muscle tension error if the muscle model is used in the simulation. The position error of the muscle starting and end points in the muscle model cause the error of the muscle tension estimation results.

Human modeling is generally considered to be difficult.

The method for the direct measurement of the geometry parameters, such as joint position or link length, is available. However, experienced techniques are required. The mechanical parameters may be measured using the corpses cutting method, but a direct measurement is impossible in a living state. CT scan and MRI technology modeling is essential for the creation of a detailed musculoskeletal model, but using it for the purpose of individual modeling is not realistic because of the cost increase. The individual model parameter estimation method intended for simple models has also been propose [25]. As regards the geometric parameter identification technique, the

calculation of the link length by the inverse kinematics solver using motion capture data is a simple measurement method [26]. The real-time identification method using a visual feedback has been proposed for the dynamic parameters [7]. However, the method of the high-DOF musculoskeletal model is absent. Hence, simple and practical modeling techniques are required.

1.2.2 Applicable fields of the musculoskeletal motion analysis

The quantification and visualization of motor skills based on the development of large-scale dynamics computations[33] and techniques of the somatosensory measurement have become available in recent years [16, 39, 17, 30]. The method for high-speed inverse kinematics and inverse dynamics calculation reduces the calculation time [9][8]. Hence, more motion data have recently been analyzed. This motion analysis simulator is used for applications in various fields.

Conventionally, in the field of sports, the physical skills obtained from long-term training have to be transmitted to the next generation through trial-and-error because quantifying the movement is difficult. Accordingly, a muscle tension estimation and visualization system for a physical activity during exercise was developed using an optical motion capture system, a force plate, and EMG sensors [32]. One technique provides the subject with a real-time visualization feedback of the muscle tension estimation using a simplified human musculoskeletal model [30, 11].

Meanwhile, from the ergonomics point-of-view, the motion analysis result can be applied to the environmental assessment in a workplace. The estimation of the load to the human body in the assembly work and the simulation result have been used as a reference value of the facility design. In the medical field, there is a trend to try to apply the simulator to the rehabilitation assessment. The simulator can provide a method to directly evaluate a patient's progress.

One example shows the motion analysis of mammals. A running horse or a walking rat motion analysis is studied through the capturing motion [27]. However, neither of them performed the muscle tension analysis estimation. The invasive approach method can be significantly adopted for use in mammals. One subject that we are attracted to are laboratory mice. Mice are useful laboratory animals for biomedical

studies. These animals are classified under early Mammalia in toxicology and have a close biological relationship with humans. The bifurcation on the evolutional tree from mice toward humans started 75 million years ago [48]. The homology of the two species is the reason of the mice' importance as laboratory animals. The completion of decoding the whole genome for mouse and human was declared in 2002 and 2003, respectively. The two species are reported to have 90% of genome in common and show 70% homology in their phenotypes [48]. The whole database, including the mouse genome, has been made available in the WEB as the Mouse Genome Informatics [1]. The recent development of a genetically modified mouse and the low cost of breeding and managements in laboratories have increased the importance of laboratory mouse as a model animal for studies in medical and pharmaceutical fields [23]. In genetic disorders, transferring knowledge from mouse experiments to humans is considered a useful approach.

The phenotype observation is commonly done for cell development and social behaviors of individual mice. More quantitative observations are of critical importance for the biomechanical evaluation of the musculoskeletal system. Technological developments are most demanded for such qualitative biomechanical observations of laboratory mice.

Many publications released studies on the modeling and analysis of the human musculoskeletal system based on the rich accumulation of anatomical and physiological knowledge [12, 24]. Nakamura et al. developed the whole-body model of the human musculoskeletal system that is appropriate and consistent with the algorithms of robotic kinematic and dynamic computation [31, 32, 34]. They also proposed an optimization algorithm to estimate muscle activities based on the information from a motion capture system and other sensory systems. Their model is one of the most detailed human musculoskeletal models in the world. The human anatomical knowledge is rich. Hence, there is an advantage for model creation.

Meanwhile, only a few studies in the literature have focused on the mouse skeletal system[10]. Little research has been done and published as regards the musculotendinous system modeling of mouse and other mammalian animals. As it is done for humans, MRI and CT imaging are the main sources of anatomical information. The MRI imaging resolution depends on the relative scale of animals and excitation

coils. Therefore, MRI imaging faces technical difficulties when it comes to small animals. Oota et al. [36, 37] more recently developed the skeletal system model of a laboratory mouse based on X-ray CT scanning. However, the modeling of the whole musculotendinous system remains to be a future problem. A practical and convenient modeling technique is required for mouse muscle modeling.

1.3 Composition of chapters

This dissertation consists of eight chapters. In Chapter 2, a mapping method for modeling the musculoskeletal system based on the skeletal geometric information is presented. Using the mapping function obtained from the homology of geometric information, wire muscle models can be transmitted to the targeted skeletal system based on the large amount of accumulated anatomical knowledge of human muscle models. We assume that the bone shape information based on Mechanostat theory preserves the stress originating from the muscle placement. First, a musculoskeletal model is introduced. To obtain the mapping function, we propose the use of SSD (Skeletal Subspace Deformation). This method obtains the mapping function from multiple feature points in the skeletal system. A weight map function, which is calculated from the distance between the muscle model and the feature points, is provided. Muscles, tendons, ligaments, and cartilage that can be modeled by the start and end points on a skeletal bone can be transmitted only from the feature points of the associated link. A virtual link that describes the branching of muscles is mapped from the mapping function formed from multiple surrounding links. The method presented in Chapter 2 is able to provide a musculoskeletal model for a human, other mammals, or even extinct animals since the mapping function is created from geometric skeletal models. The proposed method cannot present a perfect solution for the creation of new musculoskeletal modeling but can improve the modeling efficiency. In Chapter 3, the identification of the geometric and inertial parameters for a subject-specific model using body-geometry polygonal models is presented. There exists a method for identifying the kinematic or inertial parameters of lower–degrees-of-freedom (DOF) human figures up to 15 segments, does not for the larger- DOF musculoskeletal system. For extending the lower-DOF model, an identification process that uses a time series of

the motion data is presented. As an attempt to increase the estimation accuracy of the inertial parameters, the parameters are calculated beforehand on the basis of a geometric polygonal model found in database. Subject-specific kinematic parameters are identified by solving for the introduced inverse-kinematic time-invariant variables, which is the link length. The base parameter of the kinematically identified model for each link is obtained by a sequential identification method [7, 45, 5, 47, 46, 6]. The subject-specific inertial data can be estimated by the sum of the mass points arranged at regular intervals inside the body shape obtained from database. Furthermore, a weight map function obtained from the distances between distributed mass points and body links is introduced. Using the weight map proposed in Chapter 2, the deviation in the mass parameters for the spine links could be reduced. The inertial parameters are calculated using a quadratic programming method satisfying the conditions of the base and inertial parameters obtained previously. The obtained results are all of the inertial parameters that satisfy the physical consistency of the parameters. The experimentally measured data related to the force acting on the base link and the force calculated from the identified inertial model are compared to validate the identified model. The proposed method can provide simple subject identification method since the required reference motion data are one. In Chapter 4, the optimization problem for estimating the muscle tension is presented. The contact force is an important issue in dynamics simulation for estimating the joint torque and muscle tension. A contact estimation policy is classified according to the force measurement objects, and estimation for an individual case is discussed. An overview of a method for estimating the muscle tension that includes the inverse kinematics, simple contact-force estimation, and muscle-tension estimation using inverse dynamics is presented. The redundancy problem for contact-force estimation for the case where there are multiple unknown contacts is detailed. Moreover, the simultaneous optimization problem for multiple unknown contact forces and whole-body muscle-tension estimation is newly proposed. We propose a method to cope with the redundancy problem by using EMG information and limiting the direction of the force at the contact point. Thus, an analysis of contact sports becomes possible. The proposed method can also be applied to the musculoskeletal system to understand multiple contact forces from only outside observation. In Chapter 5, the dynamics simulation results based on the

method presented in Chapter 4 using the identified subject-specific model based on the method presented in Chapter 3 are analyzed. Chapter 5 also presents the results of an analysis of experts' motions using the generated individual musculoskeletal model described in Chapter 4. For the calculation, the method introduced and proposed in Chapter 4 is applied to each case. We cover elite athletes' motions that have not been quantified and visualized so far (Tai Chi, tap dance, drum performance, and internal contact force in judo). Methods for measuring the somatosensory signals by EMG and the floor reaction forces as well as the motion capture system are described. The data for the COG, joint angle, contact force, muscle activity, and muscle tension are analyzed, and the characteristics of the data are described. By understanding the actions of elite players, a greater understanding of the motions for these technique can be obtained. Chapter 6 describes a systematic method for building a musculotendinous model of a mammal—specifically, a laboratory mouse. This approach relies on the homology between mammalian species. The proposed method consists of two consecutive steps. The first step is to find a geometric morphing map from one bone of the human skeletal system to the corresponding bone of another mammalian species—namely, a laboratory mouse. The second step uses the geometric morphing maps of bones to transfer the terminal and via points of the elements of the human musculotendinous system to those of the mouse musculotendinous system. A motion capture experiment for natural walking motion is conducted. Inverse kinematics are incorporated by using the obtained mouse musculoskeletal model. The results of a muscle length analysis of the motion capture data of a mutant hairless mouse are presented. In Chapter 7, the setup for the dynamics analysis, which includes the development of force-measuring stairs and the identification of the inertial parameters of mice, is presented. The mass is identified with an approximation of the mass points distributed inside the mouse-skin geometric model. We create a staircase for a mouse that can measure the force during walking. Motion measurement including synchronized force measurement by motion capture is performed. A muscle-tension analysis of a hugger mouse, a mutant mouse, is performed, and the results are presented. The proposed method provides a simple screening measurement and a basis for evaluating detailed motor functions. The concluding remarks are given in Chapter 8.

Chapter2

Subject Specific Musculoskeletal Modeling Based on Geometric Morphing of a Skeleton

2.1 Introduction

In a motion analysis simulator including human muscle function, a musculoskeletal model is required. The model developed by Nakamura [32] is one of the most detailed musculoskeletal models in the world. The skeleton of this model has 53 grouped bone models and 155 degrees of freedom. A total of 1206 elements including 997 muscles attached to the skeleton, are arranged. Since abundant knowledge has been accumulated so far, a musculoskeletal model is often created by relying on multiple literature sources and is created by the process of carefully defining the start, end, and via points of a muscle for the skeleton, which are obtained beforehand from CT/MRI image scans. Since the muscle placement is checked individually, there is the advantage that the model can be created while checking the function of each muscle [2]. However, it is not realistic to create a large number of models tailored to subjects because of the cost. As described in the previous chapter, it is considered that the bone shape implicitly includes functional information including applied stress.

1. It is a method for obtaining a muscle model at once by creating a spatial mapping function from the bone shape of the mapping source and the mapping destination.

2. On the basis of representative data for individuals, we obtain the musculoskeletal model by fine-tuning using the geometric and dynamic parameter identification method obtained from the motion data.

The model parameters obtained by an optimization calculation based on the motion data will be described in detail in the next chapter.

The following sections are to be appeared in the publication (in preparation).

Chapter3

Subject Specific Inertia Modeling Based on Geometric Morphing of Skin

3.1 Introduction

This chapter describes a kinematic and inertial parameter identification technique for the musculoskeletal model. Kinematic parameters define the link lengths of the skeletal system and the markers used for inverse kinematics. Inertial parameters representing the mass, center of gravity, and inertia tensor are used in the dynamics simulator. Recent years have seen the proposal of human dynamics simulators based on kinematics and dynamics computation techniques developed in the field of robotics [16, 30, 32]. Since parameter errors in the musculoskeletal model affect the precision of the calculated result, those parameter errors should be minimized. If kinematic parameters cannot be estimated correctly, the generalized coordinates obtained from inverse kinematics cannot be described naturally. Likewise, incorrect estimation of inertial parameters leads directly to calculation errors of the joint torque. In cases in which the muscle model is introduced as an entity of the actuator, these parameter errors affect the result of muscle tension estimation.

Human modeling is not easy. Specifically, kinematic and inertial parameters of the human body are difficult to measure directly. A CT scan or MRI is required to create a detailed model; however, the cost of such scans means that it is unrealistic to scan every subject to create individual models. To overcome this problem, estimation methods for subject-specific modeling using a lower–degree-of-freedom (DOF) model

have been proposed [25]. To identify kinematic parameters, obtaining link lengths by solving the inverse kinematics from motion capture data is straightforward [26]. A real-time identification technique using visual feedback has been proposed for the identification of the inertial parameterscite [7].

In this chapter, we apply these technologies to propose a method for estimating the kinematic and inertial parameters for subject-specific musculoskeletal modeling using body shape information. First, link length is identified by solving the inverse kinematics and introducing time-invariant parameters. Second, base parameters are ascertained via a sequential identification method [7]. Third, using statistically estimated body shape, inertial parameters are calculated using the sum of the distributed mass point for each segment. To estimate the inertial parameters from set of mass points, a many-to-one relationship is used to calculate the distance function between each mass point and link position. In the proposed method, one mass point gives mass and inertia to multiple neighboring links in accordance with their distance. Finally, inertial parameters are obtained by solving the quadratic programming method that minimizes the error of the identified and estimated inertial parameters, with an inequality constraint to ensure positive values for the inertial parameters. To validate the proposed method, we compare the obtained inertial parameters calculated using different weighting mapping functions as reference inertial parameters. Additionally, we present the cross-validation results on external forces recalculated from the identified inertial parameters and a measured force acting on the base link.

3.2 Kinematic and Inertial Parameter Identification for a Human Musculoskeletal Model

3.2.1 Outline of Kinematic and Inertial Parameter Identification

In this study, we use the detailed human musculoskeletal model proposed by Nakamura et al [32]. Bone is modeled as a rigid body and each joint is modeled as either spherical or revolute. Assume that the muscle, as the entity of the driving joint, is

modeled as a massless wire, and that the mass of the model is concentrated on each link. The purpose of the proposed identification method is to find the rigid body parameters that describe the whole body.

Figure 3.1 shows an outline of the proposed method for identifying kinematic and inertial parameters. A time series of marker data and floor reaction force measured by an external force marker trajectory motion capture system is the input of the proposed method, which consists of the following five steps.

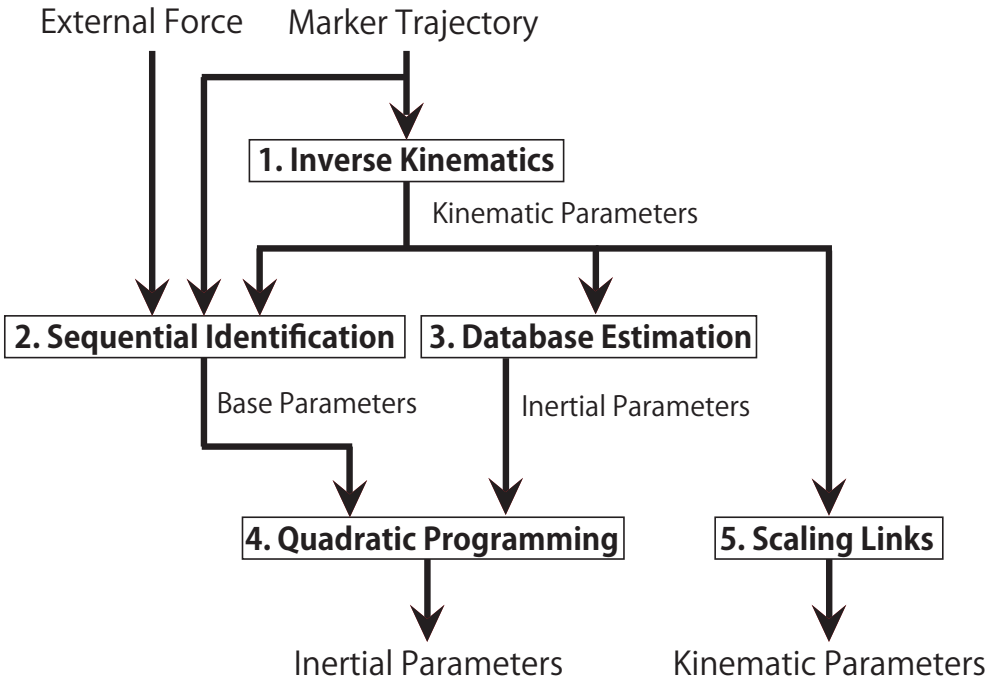

Figure 3.1: Outline of the proposed method to identify kinematic and inertial parameters

1. *Identification of kinematic parameters by solving the inverse kinematics:* We use the kinematic parameter identification method proposed by Ayusawa et al [26]. In this method, introducing virtual prismatic joints—the distance between human body joints as virtual generalized coordinates—results in the inverse kinematics problem. The kinematic identification method follows the steps below.

   (a) The result of the inverse kinematics about generalized coordinates defined

as spherical and revolute joints is set to the initial value of the generalized coordinate on each frame.

(b) By introducing additional virtual generalized coordinates to the model as time-invariant prismatic joints that describe the distance between each joint, link length can be obtained by solving the inverse kinematics for all generalized coordinates at all frames.

(c) By temporarily fixing all generalized coordinates and introducing a new generalized coordinate that describes the marker position, the position of the model marker can be determined by solving inverse kinematics.

A converged solution of link length and marker position are obtained by iteration of (b) and (c).

2. *Identification of base parameters of sequential identification method:* The base parameters of the kinematically identified model on each link is obtained by sequential identification method. Base parameters are the set of inertial parameters dependent on the joint structure of the model, obtained by deleting redundant parameters in the equation of motion. For more information about the sequential real-time identification method, see [7]. This method utilizes the identifiability of any chained rigid body based only on information about the base link motion and external force.

3. *Estimation of inertial parameters using statistical data:* Subject-specific inertial data can be estimated using the sum of the mass point arranged at regular intervals in the body shape obtained from the database. Assume that a rigid body is constituted by mass points, which are closest to the center of gravity (COG) of the link. The Body Shape Browser, created by Ergo Vision Co., Ltd., was used to create our subject-specific model. Operating parameters to form the body shape were determined by principal component analysis based on scanned and measured data at the Digital Human Research Center National Institute of Advanced Industrial Science and Technology. In this study, we acquired an initial subject model using height and chest circumference.

4. *Calculation of inertial parameters by quadratic programming:* Inertial parameters are obtained by solving quadratic programming that satisfies the conditions of the base and inertial parameters obtained from steps 2 and 3, respectively.

5. *Applying the kinematic parameters of the lower-DOF model to the high-DOF musculoskeletal model:* Kinematic parameters obtained from step 1 are applied to the high-DOF model. The distance between joints applies to corresponding segments of the high-DOF model. Joint position in the lower-DOF model is equal to the corresponding joint position in the high-DOF model.

In the next section, steps 3 and 4 are explained in detail.

3.2.2 Identification of inertial parameters

The equation of motion of a rigid body can be described as follows, using identifiable base parameters $\boldsymbol{\phi}_B$ [28].

$$\boldsymbol{Y}_B\boldsymbol{\phi}_B = \boldsymbol{f}, \tag{3.1}$$

$$\boldsymbol{\phi}_B = \boldsymbol{Z}\boldsymbol{\phi}. \tag{3.2}$$

Equation (3.1) is the equation of motion transformed linearly, where $\boldsymbol{Y}_B$ is a regressor matrix related to $\boldsymbol{\phi}_B$, and $\boldsymbol{f}$ describes generalized force.

$\boldsymbol{\phi} \in \boldsymbol{R}^{10N_J}$ describes the inertial parameters, and consists of vector $\boldsymbol{\phi}_i$, which are inertial parameters of each link:

$$\boldsymbol{\phi} = [\boldsymbol{\phi}_1 \quad \boldsymbol{\phi}_2 \quad \dots \quad \boldsymbol{\phi}_{N_J}]^{\mathrm{T}} \in \boldsymbol{R}^{10N_J}, \tag{3.3}$$

where N_J is the number of joints, $\boldsymbol{Z}$ is a restructured matrix determined by link structure, and $\boldsymbol{\phi}_i \in \boldsymbol{R}^{10}$ is a vector consisting of 0th-,1st-, and 2nd-order moments.

$$\begin{aligned}\boldsymbol{\phi}_i = [&m_i \quad m_i c_{i,x} \quad m_i c_{i,y} \quad m_i c_{i,z} \\ &I_{i,xx} \quad I_{i,yy} \quad I_{i,zz} \quad I_{i,yz} \quad I_{i,zx} \quad I_{i,xy}]^{\mathrm{T}},\end{aligned} \tag{3.4}$$

where m_i is the mass of the ith link, $c_{i,x}, c_{i,y}, c_{i,z}$ are members of COG position c_i described from the ith link coordinate, and $I_{i,xx}, I_{i,yy}, I_{i,zz}, I_{i,yz}, I_{i,zx}, I_{i,xy}$ are members of inertia matrix $\boldsymbol{I}_j \in \boldsymbol{R}^{3\times3}$ around the coordinate origin of the ith link.

Let us assume that the whole rigid body consists of N_P mass points. Each mass point has a constant mass value and one-to-one correspondence with a rigid body. Inertial parameters of a rigid body can be described as follows using mass vector $\boldsymbol{\rho}^{ref} = \{\rho_j^{ref}\} = \begin{bmatrix}\rho_1^{ref} & \rho_2^{ref} & \dots & \rho_{N_P}^{ref}\end{bmatrix}^{\mathrm{T}} \in \boldsymbol{R}^{N_P}$:

$$\boldsymbol{\phi}^{ref} = \hat{\boldsymbol{W}}\boldsymbol{\rho}^{ref}. \tag{3.5}$$

Coefficient matrix $\hat{\boldsymbol{W}} \in \boldsymbol{R}^{10N_J \times N_P}$, which relates the vector mass and mechanical parameters, is defined as follows:

$$\hat{\boldsymbol{W}} = \boldsymbol{W} \circ \boldsymbol{V}, \tag{3.6}$$

where $\boldsymbol{W} \in \boldsymbol{R}^{10N_J \times N_P}$ is a weighting matrix that represents the contribution of the mass to each rigid body, and $\boldsymbol{V} \in \boldsymbol{R}^{10N_J \times N_P}$ is a matrix consisting of inertial parameters normalized by mass. The elements of matrices $\boldsymbol{W}$ and $\boldsymbol{V}$ are composed of 10-dimensional column vectors $\boldsymbol{W}_{ij}$ and $\boldsymbol{V}_{ij}$, defined below.

$$\begin{aligned}\boldsymbol{W} &= \{\boldsymbol{W}_{ij}\},\ \boldsymbol{W}_{ij} \in \boldsymbol{R}^{10},\\ \boldsymbol{V} &= \{\boldsymbol{V}_{ij}\},\ \boldsymbol{V}_{ij} \in \boldsymbol{R}^{10},\end{aligned} \tag{3.7}$$

$$\boldsymbol{W}_{ij} = w_{ij}\left[1\ 1\ \dots\ 1\right]^{\mathrm{T}}, \tag{3.8}$$

$$\begin{aligned}\boldsymbol{V}_{ij} = [1\ &r_{ij,x}\ r_{ij,y}\ r_{ij,z}\ r_{ij,y}^2 + r_{ij,z}^2\ r_{ij,z}^2 + r_{ij,x}^2\\ r_{ij,x}^2 + r_{ij,y}^2\ &- r_{ij,y}r_{ij,z}\ - r_{ij,z}r_{ij,x}\ - r_{ij,x}r_{ij,y}]^{\mathrm{T}}.\end{aligned} \tag{3.9}$$

w_{ij} is a weighting constant of the jth mass point related to the ith link, which is often defined by a distance function, and can have any form under the condition $\sum_{i=1}^{N_J} w_{ij} = 1$. $r_{ij,x}, r_{ij,y}, r_{ij,z}$ represents the elements of the position vector to the jth mass point as seen from the ith link.

Thus, $\boldsymbol{\rho}$ is derived as the solution of the quadratic programming below:

$$f(\boldsymbol{\rho}) = \frac{1}{2}W_\phi|\boldsymbol{\phi}_{base}^{ref} - \boldsymbol{Z}\hat{\boldsymbol{W}}\boldsymbol{\rho}|^2 + \frac{1}{2}W_\rho|\boldsymbol{\rho} - \boldsymbol{\rho}^{ref}|^2$$
$$s.t. \quad \rho_j > 0. \tag{3.10}$$

The first term in the formula describes the evaluated value of identified base parameters $\boldsymbol{\phi}_{base}^{ref}$. The second term describes the evaluated value of all reference mass points in vector ρ^{ref} to the body shape database set. To solve the quadratic programming introducing above, values of distributed mass points $\boldsymbol{\rho}$ are obtained. The obtained inertial parameters always satisfy the physical conditions that $\rho_j > 0$.

The reference values of mass points $\boldsymbol{\rho}^{ref}$ are constant, and can be described as $\boldsymbol{\rho}^{ref} = \{\rho^{ref}\}, \rho^{ref} = M/N_p$ using the total mass of the rigid body of system M. The weight parameters W_ϕ and W_ρ in the quadratic programming can be set based on the reliability of the measured base parameters or all inertial parameters calculated from the body shape database. The above equation can be reduced to a general constrained quadratic programming problem by deformation.

$$f(\boldsymbol{\rho}) = \frac{1}{2}\boldsymbol{\rho}^{\mathrm{T}}\boldsymbol{A}\boldsymbol{\rho} + \boldsymbol{b}^{\mathrm{T}}\boldsymbol{\rho}, \quad s.t. \;\; \rho_j > 0, \tag{3.11}$$

where

$$\boldsymbol{A} = W_\phi(\boldsymbol{Z}\hat{\boldsymbol{W}})^{\mathrm{T}}\boldsymbol{Z}\hat{\boldsymbol{W}} + W_\rho E, \tag{3.12}$$
$$\boldsymbol{b} = -W_\phi(\boldsymbol{Z}\hat{\boldsymbol{W}})^{\mathrm{T}}\boldsymbol{\phi}_{base}^{ref} - W_\rho\boldsymbol{\rho}^{ref}. \tag{3.13}$$

In the experiment described in the next section, the two types of weight parameter w_{ij} in (3.8) are designed and compared with the obtained mass parameters.

1. *Weight map as the function of the distance between the link COG and mass points:*

$$w_{d,ij} = \frac{|\boldsymbol{p}_{ij}|^{-4}}{\sum_{i=1}^{N_J}|\boldsymbol{p}_{ij}|^{-4}}. \tag{3.14}$$

$\boldsymbol{p}_{ij}$ is the COG position of the ith link referred from the coordinate of the jth mass point. Introducing weight map $w_{d,ij}$ may describe the mass parameters of deformable body segments.

2. *Weight map obtained from one-to-one correspondence between rigid body link and mass point:*

$$w_{n,ij} = \begin{cases} 1 & \left(|\boldsymbol{p}_{ij}| = \underset{1 \le i \le N_J}{\operatorname{argmin}} |\boldsymbol{p}_{ij}|\right) \\ 0 & (otherwise) \end{cases} \tag{3.15}$$

The weight map $w_{n,ij}$ describes that each mass points gives inertial parameters to the nearest rigid body links. All inertial parameters obtained from the two types of weight function are described by $\boldsymbol{\phi}_{w_d}$ and $\boldsymbol{\phi}_{w_n}$, respectively.

3.3 Experiment for identification of kinematic and inertial parameters

The optical motion-capture system was used to measure human motion. The positions of the 34 optical reflective markers pasted on the whole body were recorded by 10 motion capture cameras (Motion Analysis Corporation) at 200 fps. At the same time, the external force applied to the body was measured at 1000 fps using a force plate (Kistler Japan Co., Ltd). The subject was an adult male with 182.2 cm height, 66.8 kg weight, and 87.0 cm chest circumference. It is desirable to excite all the body joints for the identification of motion. The progress of their identification at the time of measurement were fed back to the subjects using a visualization application [7].

Figure 3.2 shows the model used in this experiment. The left-hand side depicts the lower-DOF model and its joint placement and the large-DOF model (53 links, 155 DOF) and its body shape model. The lower-DOF model was equal to the corresponding joint position of the large-DOF model. In identifying the kinematic parameters, we introduced 14 prismatic joints as time-invariant generalized coordinates between the joints. The inertial parameters were obtained in advance using the body shape information shown in Fig. 3.2. To that end, the initial posture of the body shape model and the skeletal model needs to be matched. An initial model was obtained by fitting the skeletal model to the body shape model by solving the inverse kinematics used in the kinematic identification targeted to the body shape model obtained from the height and the chest with virtual markers (same as the 34-measurement marker

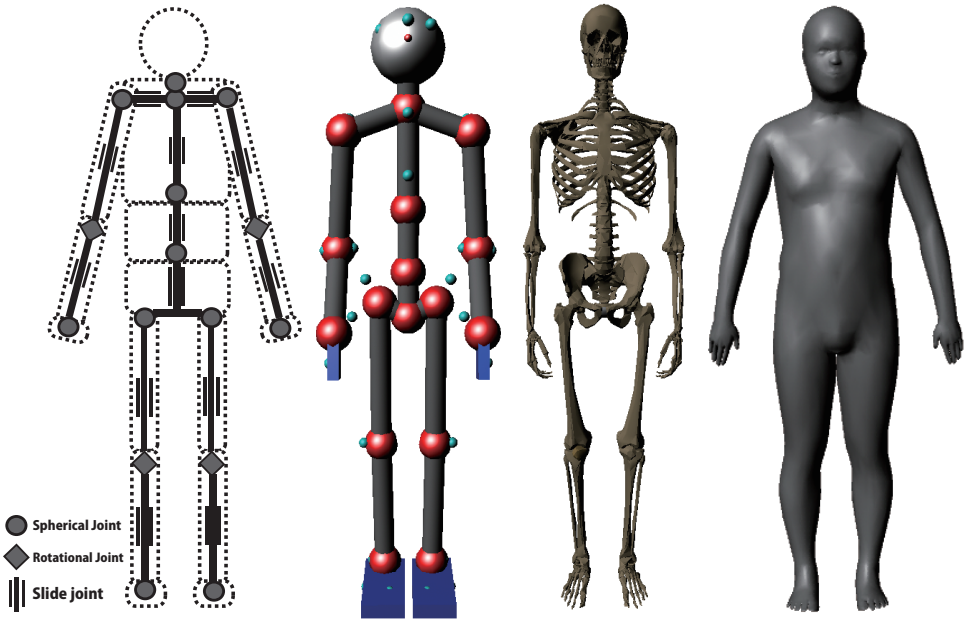

Figure 3.2: Model overview: (from the left-hand side) lower-DOF joint definition (18 links, 40 DOF (excluding 14 prismatic DOFs)), and its model (34 markers) and the large-DOF skeletal model (53 links, 155 DOF) and its body shape.

placement). The subject-specific model can be estimated by applying the kinematic parameters obtained earlier. The points defined in the muscle model described the relative position from the position of the joint centers. Hence, the kinematic parameter identification created subject-specific muscle models at the same time. A mass point was placed inside the subject-specific model in a grid at 5-mm intervals. The inertial parameters were then obtained. For the calculation of the inertial parameters, the initial posture of the model was set to open hands and legs to avoid an unnatural interference between the segments. The kinematic parameters were identified using 50 frames of marker data. The contact forces measured by the force plates were used as an input for the sequential identification method [7]. The 180 s motion data (36,000 frame data) were used to identify the base parameters. The weight parameters W_ϕ and W_ρ for the optimization of Eq. (3.10) were set as 1.

3.4 Result of the inertial parameter identification

Tables 3.1 and 3.2 show the identification result of the mass parameters used to extract all the inertial parameters. The left-hand side of the table presents the following column values: 1) identified mass m_{w_d} using the weighted map w_d; 2) identified mass m_{w_n} using the one-to-one mass point weight map; and 3) calculated mass only from the distributed mass points to the database body shape m^{ref} using the constant value of the mass point. Note that the mass point values in the identification results were not constant values because each mass points' value was the target to be optimized.

Table 3.1: (1/2) Comparison of the mass [kg]: (from the left-hand side) 1) identified mass $\boldsymbol{\phi}_{w_d}$ using the weighted map w_d; 2) identified mass $\boldsymbol{\phi}_{w_n}$ using the one-to-one mass point weight map; and 3) calculated mass only from the distributed mass points to the database body shape ϕ^{ref} using the constant value of the mass point.

Link	1) m_{w_d}[kg]	2) m_{w_n}[kg]	3) m^{ref}[kg]
Pelvis	5.43	6.72	10.72
Lumber vertebra 5	2.85	3.07	3.39
Lumber vertebra 4	2.12	1.87	1.89
Lumber vertebra 3	1.80	1.83	2.17
Lumber vertebra 2	1.67	1.79	2.00
Lumber vertebra 1	1.61	1.22	1.72
Rib vertebra 12	1.54	1.58	1.33
Rib vertebra 11	1.48	2.29	1.50
Rib vertebra 10	1.25	0.83	0.67
Rib vertebra 9	1.16	1.45	1.28
Rib vertebra 8	1.26	1.88	1.28
Rib vertebra 7	0.97	0.67	0.61
Rib vertebra 6	0.90	0.64	0.56
Rib vertebra 5	0.85	0.58	0.44
Rib vertebra 4	0.76	0.43	0.28
Rib vertebra 3	0.73	0.77	0.67
Rib vertebra 2	0.61	0.57	0.56
Rib vertebra 1	0.48	0.09	0.22
Neck vertebra 7	0.42	0.30	0.39
Neck vertebra 6	0.39	0.12	0.11
Neck vertebra 5	0.41	0.21	0.44
Neck vertebra 4	0.44	0.02	0.11
Neck vertebra 3	0.59	0.35	0.50
Neck vertebra 2	0.77	0.12	0.22
Neck vertebra 1	1.32	2.29	2.17
Head	0.93	1.35	0.83

Table 3.2: (2/2) Comparison of the mass [kg]: (from the left-hand side) 1) identified mass $\boldsymbol{\phi}_{w_d}$ using the weighted map w_d; 2) identified mass $\boldsymbol{\phi}_{w_n}$ using the one-to-one mass point weight map; and 3) calculated mass only from the distributed mass points to the database body shape ϕ^{ref} using the constant value of the mass point.

Link	1) m_{w_d}[kg]	2) m_{w_n}[kg]	3) m^{ref}[kg]
Right shoulder clavicle	0.57	0.53	0.50
Right shoulder blade	1.04	1.16	1.11
Right upper arm	1.87	2.05	1.28
Right forearm ulna	1.16	1.30	0.94
Right forearm radius	0.65	0.51	0.33
Right hand	0.34	0.34	0.11
Left shoulder clavicle	0.50	0.35	0.33
Left shoulder blade	1.09	1.30	1.22
Left upper arm	1.72	1.90	1.22
Left forearm ulna	0.96	1.13	0.83
Left forearm radius	0.58	0.41	0.28
Left hand	0.40	0.40	0.22
Chest	1.09	0.33	0.33
Right cartilago rib	0.83	1.17	1.44
Left cartilago rib	0.86	1.16	1.44
Right leg thigh	4.29	3.73	5.55
Right leg tibia	1.67	1.50	0.89
Right leg fibula	1.20	0.97	0.56
Right foot	1.37	1.40	0.67
Right toe	0.22	0.4	0.22
Right kneecap	2.06	2.15	1.44
Left leg thigh	3.91	3.53	6.05
Left leg tibia	1.72	1.60	1.00
Left leg fibula	1.21	1.04	0.56
Left foot	1.40	1.39	0.56
Left toe	0.33	0.53	0.22
Left kneecap	2.15	2.17	1.50
Total	67.43	67.46	66.8

Table 3.3 shows the standard deviation of the mass parameter in the spine link groups. The standard deviation among the mass of the spine links in the identified results using the weight map w_n was less than that of the weight map w_d. The variation calculated by the weight map w_d showed discreteness because of the mass point estimation. Meanwhile, the results on the weight map w_d described the absorbance of the mass variation of the neighboring links. The weight design w_d described the human model well, especially the segments that included the deformable bodies, because the variation was less.

Table 3.3: Standard deviation of the spine link mass [kg]

Link group	σ_{w_d}[kg]	σ_{w_n}[kg]	σ^{ref}[kg]
Lumbar vertebras	0.46	0.60	0.60
Rib vertebras	0.32	0.63	0.42
Neck vertebras	0.31	0.75	0.63

Table 3.4: Comparison of the proportion of the segment mass to the total mass of the whole body [%] (the data are from the right side of the body, except the head and the trunk): (from the left-hand side) the segment mass of the Japanese male athlete [3] identified mass using the weight map w_d, identified mass using the weight map w_n, and calculated mass only from the distributed mass points to the database body shape ϕ^{ref} using the constant value of the mass point.

Segment	Body mass[3] [%]	m_{w_d}[%]	m_{w_n}[%]	m^{ref}[%]
Head	6.9	7.79	7.05	6.98
Body	45.9	48.88	50.81	56.36
Upper arm	2.7	2.77	3.03	1.91
Lower arm	1.6	2.69	2.68	1.91
Hand	0.6	0.51	0.51	0.17
Thigh	11	6.36	5.52	8.31
Shank	5.1	4.26	3.67	2.16
Foot	1.1	2.36	2.67	1.00
Upper body	30.2	25.93	26.36	23.61
Lower body	18.7	22.95	24.45	32.75

Table 3.5: Corresponding table for the segment names on the Japanese athlete model [3] and the link names on Nakamura's model.

Segment name used in Table 3.4	Link name on Nakamura's model
Head	Head, Neck vertebra 1-5
Body	Rib Vertebra 1-12, Clavicles, Shoulder blades, Chest, Cartilago ribs Pelvis, Lumber vertebra 1-5
Upper arm	Upper arm
Lower arm	Fore arm ulna, Forearm radius
Hand	Hand
Thigh	Leg thigh
Shank	Leg tibia, Leg fibula, Kneecaps
Foot	Foot, Toe
Upper Body	Rib vertebra 1-12, Clavicles, Shoulder blades, Chest, Cartilago ribs
Lower body	Pelvis, Lumber vertebra 1-5

Table 3.4 shows the comparison result of the mass distribution of the Japanese male athlete [3] and identified the results in percentage. The identification result calculated using the weight map w_d was close to that of the athlete's results. The mass values of the shank and the foot were slightly different. However, the sum of the shank and the foot in the identified results was close to that of the athlete's because of the design of the weight function using the position of COG being nothing but a joint position.

Moreover, the mass of the kneecap seemed to be much larger than that shown in Fig. 3.2. The calculation of all the inertial parameters using the body shape information showed that some of the lower thigh mass were absorbed because of the COG calculation of each link. However, the resultant force calculated in the dynamics simulator did not have much effect because no DOF is usually provided to the kneecap bone. This finding was also observed in the neck vertebra to the head and the pelvis to the lumbar vertebra 5.

Figure 3.3 shows the comparison of the measured force and the force calculated from the identified inertial parameter and the force calculated from the body shape model. In the figure, the thin line denotes the measured force applied to the base link, while the bold line represents the force calculated from the regressor matrix

and the identified inertial parameter, $\boldsymbol{Y}_B\boldsymbol{\phi}_B$. The dotted thin line shows the force calculated from the regressor matrix and the estimated inertial parameter, $\boldsymbol{Y}_B\boldsymbol{\phi}_{ref}$. Another motion datum with the same subject was used for this cross-validation. The average error between the measured and identified forces during the 167 s motion was F_x : 0.32 [N], F_y : 0.99 [N], F_z : 0.25 [N], N_x : 1.04 [Nm], N_y : 1.20 [Nm], and N_z : 0.04 [Nm], which matched well. The estimated values from the body shape were F_x : 0.32 [N], F_y : 2.75 [N], F_z : 9.13 [N], N_x : 5.86 [Nm], N_y : 4.21 [Nm], and N_z : 2.39 [Nm], which were larger than the identified one.

Knowledge on the body composition density can possibly be used as the reference of $\boldsymbol{\rho}^{ref}$.

3.5 Summary

This study proposed the identification of the kinematic and inertial parameters of a subject-specific model using body shape information. The link length was obtained by introducing additional virtual generalized coordinates to the model as a time-invariant prismatic joint that described the distance between each joint and by solving the inverse kinematics for all the generalized coordinates at all frames. The base parameters were obtained using the sequential identification method. The subject-specific inertial data can be estimated by the sum of the mass point arranged at regular intervals for the body shape data obtained from the database. The inertial parameters were obtained by solving the quadratic programming satisfying the conditions of the base and inertial parameters. The five characteristics of the proposed method are presented as follows:

1. The proposed method can provide subject-specific parameters from the measured one motion. Hence, the simplicity of model creation was achieved.

2. All the inertial parameters can be identified, while the unidentifiable inertial parameters can be optimized from the information of the body shape obtained from the database.

3. The identified mass parameters in the spine links can be obtained under the

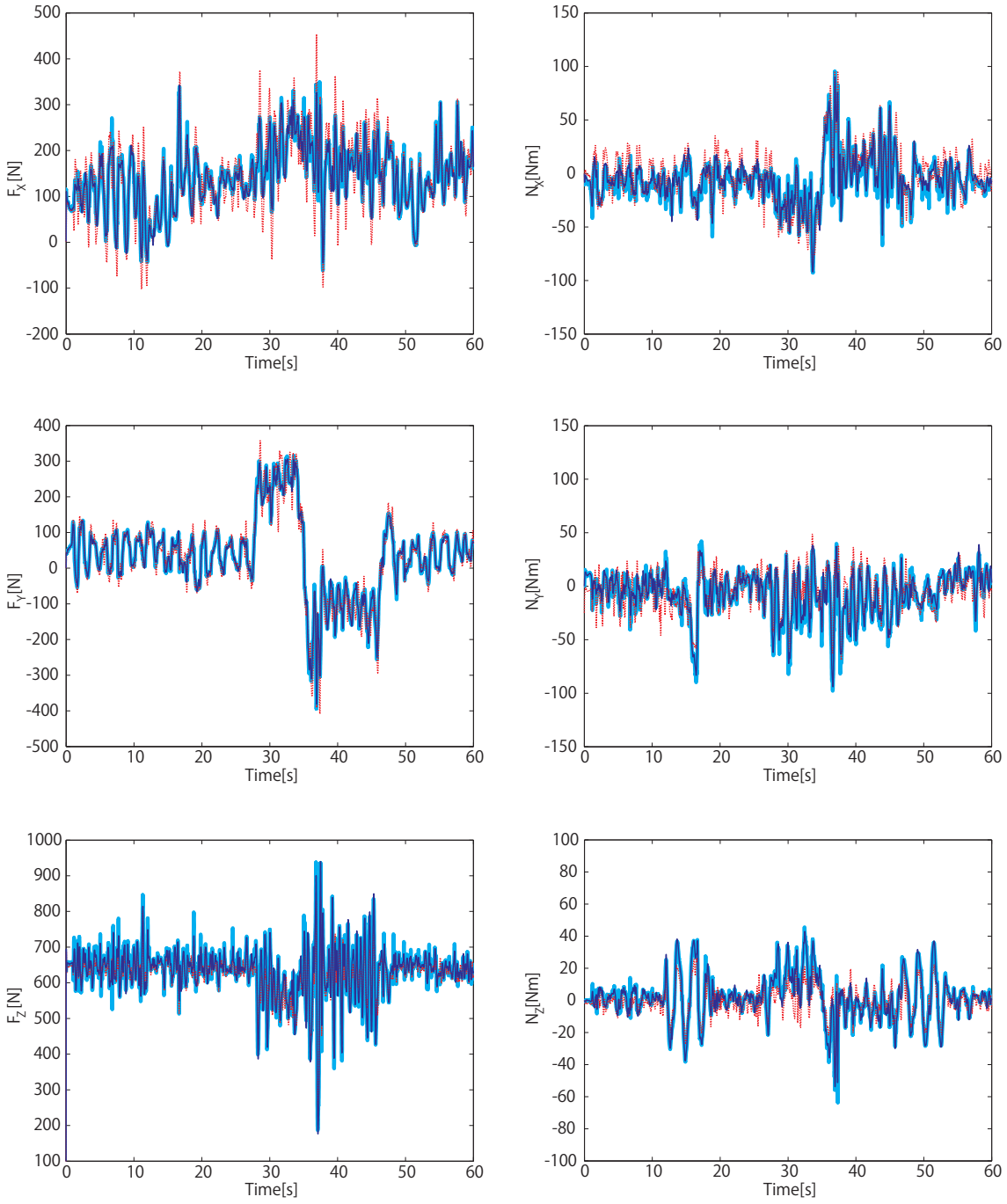

Figure 3.3: Cross-validation on the force applied to the base link: comparison of the measured force (bold line) and the force calculated from the identified inertial parameter (thin line) and the force calculated from the body shape model. The average error between the measured and identified forces during the 167 s motion is F_x : 0.32 [N], F_y : 0.99 [N], F_z : 0.25 [N], N_x : 1.04 [Nm], N_y : 1.20 [Nm], and N_z : 0.04 [Nm]. The error between the measured and estimated values from the body shape isF_x : 0.32 [N], F_y : 2.75 [N], F_z : 9.13 [N], N_x : 5.86 [Nm], N_y : 4.21 [Nm], and N_z : 2.39 [Nm].

condition of less standard deviation by introducing the weighted map for the mass point's calculation of the link mass.

4. The optimization problem of the mass points is solved with the positive constraint. The physical condition is always satisfied.

5. The subject-specific muscle model can be obtained through the parametrization of the kinematic parameters and is expected to improve the accuracy of the muscle motion analysis because the muscle is modeled by a relative value of the joint center.

A motion capture experiment was conducted to validate the proposed method. A cross-validation on the measured force and that calculated by identifying the inertial parameter was also performed. Moreover, a recreation of the reaction force was confirmed using the identified parameters. Four findings are obtained according to the inertial identified data:

1. The deviation of the spine mass can be suppressed to 0.31 to 0.46 kg in the proposed method.

2. The average error applied to the base link between the measured and identified forces during the 167 s motion is F_x : 0.32 [N], F_y : 0.99 [N], F_z : 0.25 [N], N_x : 1.04 [Nm], N_y : 1.20 [Nm], and N_z : 0.04 [Nm].

3. Some of the link masses are absorbed into the neighboring links because of the position.

Chapter4

Motion Analysis with Contact Force Estimation

4.1 Introduction

Studies on human motion analysis in the field of biomechanics have been performed concurrently with the improvement of computer resources and the development of sensing devices for somatosensory information. Especially with the advent of the musculoskeletal motion simulator, the visualization and quantitative analysis of motion skills has been positively realized, which has been technically difficult thus far [16, 17, 39].

The recent method of high speed inverse kinematics and inverse dynamics calculation drastically reduces the calculation time [8, 9], so more motion data can be analyzed. Additionally, there is a simulator that can provide muscle force estimation results in real time for a variety of motion measurements and analyses in sports biomechanics [11, 30]. Thus, it has become possible to immediately give kinematic and dynamic estimation to the experimental subject through visualization feedback. Biomechanics research in individual sports has already begun to target a wide variety of fields. In the dynamics calculation, along with the mass parameters of the simulation model, an estimation of the contact force applied to the model is also required in the simulation system.

In most musculoskeletal simulators, it is possible to run dynamics calculations to determine the contact force applied to the multibody system. Usually the reaction force measured by the force plate can be directly input into the dynamics calculation. If the contact force is unknown during the measured motion, Open Simm, which is

being developed by Delp et al. [15, 16, 42], can be used to estimate the contact force by the modeling of elastic deformation and friction of the contact point [43]; therefore, the accuracy of the contact force estimation result depends on the precision of the elasticity and friction coefficient of the model. Nakamura et al. [32], has proposed a technique for optimizing the acting contact force by solving quadratic programming to minimize the errors between the dynamic force at the floating base link and the actual reaction force data measured in the force plate data, regardless of the number of contact points.

Those musculoskeletal dynamics simulators initially estimate the contact force and subsequently optimize the muscle tension of the system. Because the simulator calculates the contact force first, the error of the contact force will affect the resultant muscle tension estimation. If the experimental setup can access the force plate data and these data are similar in number to the number of contact points, the contact force can be calculated accurately. If the number of the contact points with unknown forces increases, accurate results cannot be expected from solving the optimization problem for the estimation of all the contact forces. In those cases, it is necessary to measure or estimate the contact force at each contacting point; however, measurement interferes with or limits the motion in many situations. The contact state, which includes the number of contact points, measurement rate, and contact duration are highly dependent on each motion. Therefore, a simplified and practical measurement is needed. In this chapter, techniques for estimating the contact force in four specific situations—described in the following section—are proposed.

The following sections are to be appeared in the publication (in preparation).

Chapter5

Analysis of Masters' Skills from Musculoskeletal Estimation

5.1 Introduction

Physical skills acquired over a long period of time are transmitted to the next generation through trial and error because it is difficult to quantify movement. In recent years, on the basis of development of large-scale dynamics computation [33] and the technique of somatosensory measurement, quantification and visualization of motor skills are becoming available [16, 17, 39]. Using the subject-specific musculoskeletal model identified based on the method proposed in Chapter 3, we analyzed the motion of experts, which has been difficult to quantify and visualize previously. For the motion analyses, we also applied contact force estimation based on the previous chapter. The four motions listed below are analyzed, and the findings obtained are described:

1. Tai Chi: measurable contact force obtained from force plate
2. Tap dancing: force plate data obtained using a high-speed camera to detect contact states
3. Drum playing: contact force converted from sound
4. Judo Uchimata: simultaneous estimation of contact force and muscle tension

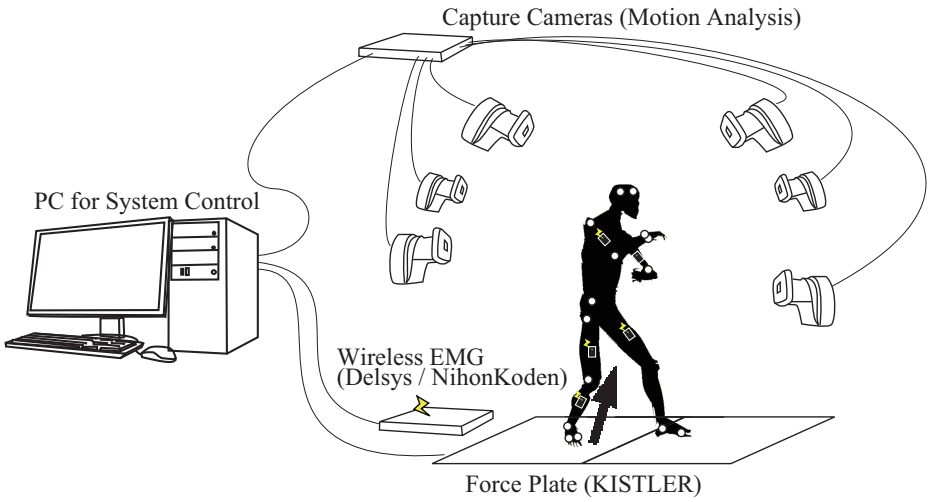

Figure 5.1: Overview of the motion capture system.

5.2 Musculoskeletal Model and Experimental Environment

This chapter deals with motion analysis, and all subject-specific musculoskeletal models are identified and used for calculations based on Chapter 3. Figure 5.1 shows the overview of the optical motion capture system, by which time series data of body marker trajectories (34 trajectories in total) are measured. Floor reactive force and surface EMG are measured simultaneously with the motion capture system using a faceplate (Japan Kistler) and wireless surface EMG sensors (Delsys, Nihon Kohden). For consideration of external force on the rigid body, the timing of contact with external environment must be known. In this study, the contact timing and joint motions are recorded by high-speed cameras (300?600 fps) synchronized with the motion capture system.

5.3 Experts' motion skills

5.3.1 Tai Chi motion

Tai Chi motion is characterized by slow and flowing movements. It is considered important to focus on the muscles of the lower limbs and to maintain a lower center of gravity (COG). Forty seconds of dance performance were analyzed. The orientation of the trunk was reversed after each 20-second or 35-second increment (right foot forward to left foot forward). Figure 5.2 shows snapshots of the calculation results of muscle tension analysis. Figure 5.3 shows changes in the position of the COG and major muscle activities during movement.

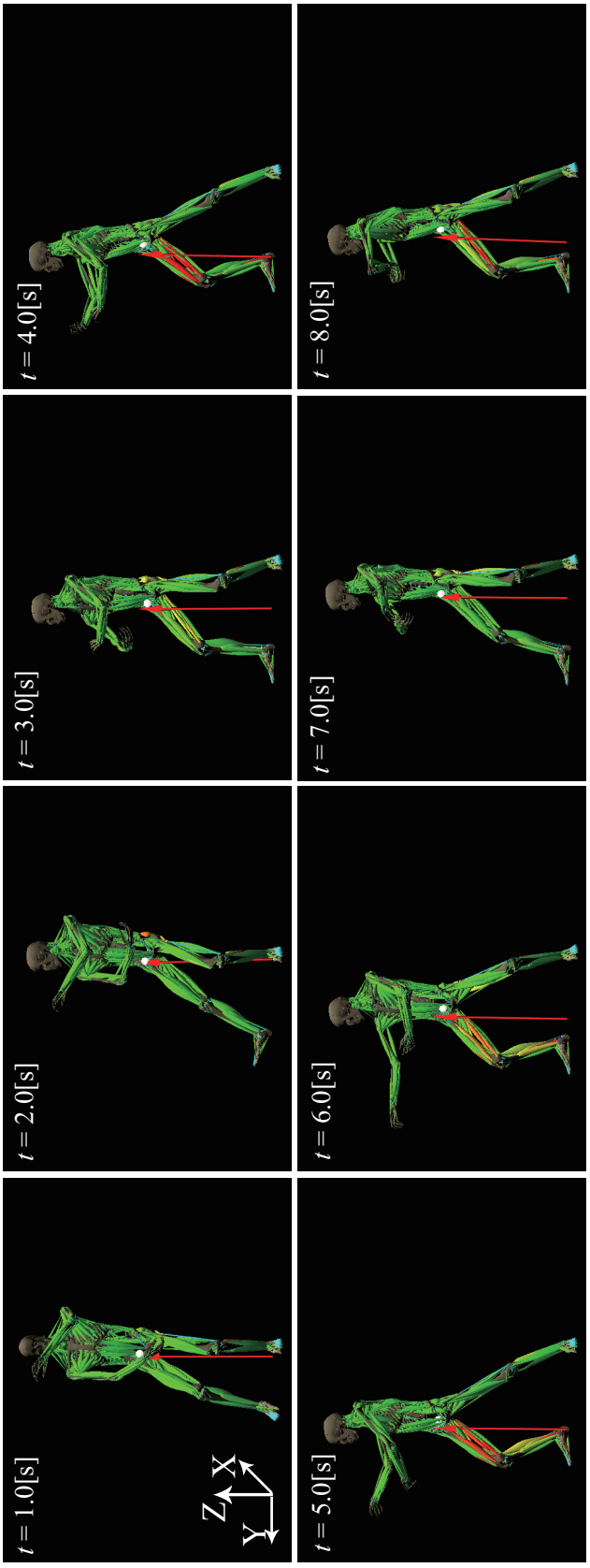

Figure 5.2: Snapshots of the TaiChi motion

The graphs show the (a) anterior deltoid, (b) posterior deltoid, (c) long head of the biceps, (d) triceps lateral head, (e) rectus femoris muscle, (f) long head of the biceps femoris muscle, (g) tibialis anterior muscle, and the (h) lateral head of the gastrocnemius muscle.

The following considerations are based on the analysis results.

- The height of the COG is low and movement is stable. The height of the COG is low compared with the standing posture, as shown in Figure 5.2. As shown in Figure 5.3, the maximum position in the Z-axis direction is 50 mm at most over 30 s, which is substantially parallel to the XY plane. Considering the lower height of the COG, the movement is very stable.

- Displacement of the COG in the axial direction Y is periodic. In each period, the COG moves from the vertical position on the right foot to the left foot, similar to walking behavior in the steady state. In addition, the periodic movement of the COG along the X-axis direction can be seen. This is because the subject orientation is reversed after 20 seconds. Eight periodic cycles can be confirmed during 40 seconds of motion. The duration of one period is about 5 s, which is rather slow compared to other movements.

- Muscles of the lower limbs work actively. There is a relationship between the periodicity of the motion of the COG in the axial direction Y and the periodicity of the motion of the rectus femoris, tibialis anterior, and gastrocnemius. The movement in the positive Y-axis direction corresponds to the muscles of the right side of the body, and negative movement corresponds to the left side of the body. The biceps femoris works for only about 20 to 35 seconds to turn the body.

- Muscles in the upper body work less compared to the muscles in the lower limbs. In particular, the triceps does not work substantially. Motion under the weaker condition is presumed. However, the deltoid and biceps work periodically, and both arms are used to move the COG. That is, the subject moves forward with both hands spread apart and moves backward with hands closed. This can be

interpreted in the sense that forward movement represents an attack movement, and backward movement represents a defense movement.

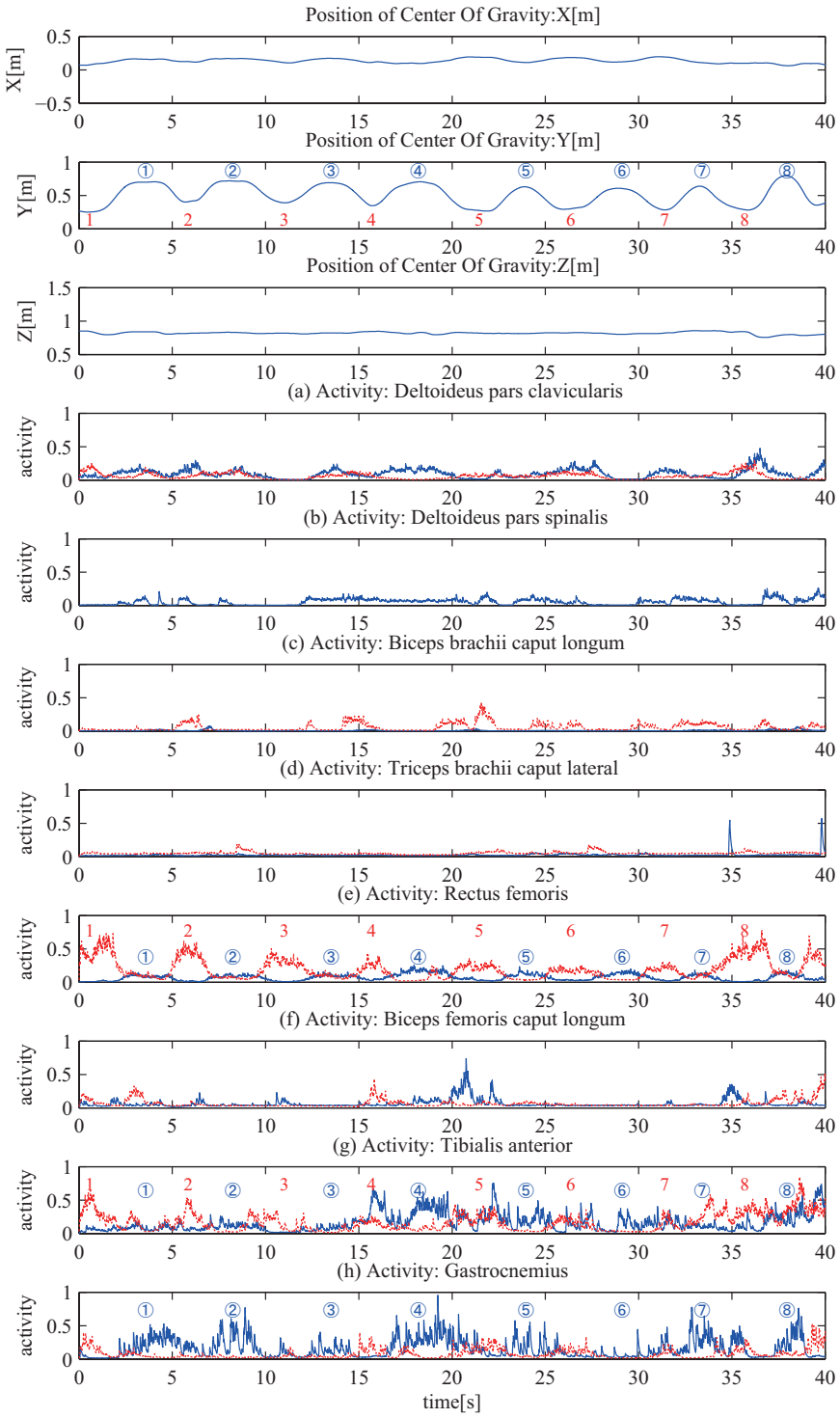

Figure 5.3: TaiChi motion: Position of the COG and activation of major muscles (Blue line shows the right side of the body, red dot shows left side of the body)

5.3.2 Tap dancing

Tap dancing is characterized by sounds initiated by contact between the floor and special shoes with metal on the toe and heel. The sound is produced by vertical motion. Twenty seconds of motion were analyzed in this study. Figure 5.4 shows snapshots of tap dancing with visualized muscle activity. Figure 5.5 shows the contact state between the foot and floor, the height of the COG, and 16 major muscle activities. In the contact state graph, each line represents a contact state between the foot and the floor. Tap dancing involves some small differences from Tai Chi motion: the (i) trapezius muscle and (j) gluteus maximus muscles are measured. The following considerations are based on the analysis results.

- The COG shows oscillatory motion in the vertical direction. The height of the COG is lower than in the standing posture, on average. The average value of the COG in the Z-axis direction was 0.883 m during the initial state over 0–0.8 s and 0.861 m (with a variance of 0.0011 [m ^{2}]) during 0.8–18 s of movement. These data imply that the subject does not only try to hit the ground with a jumping motion, but also with a COG lower than in the initial state.

- Muscles of the entire body are actively involved, in particular the upper limb muscles. The COG along the Z-axis seemed to be controlled using inertial forces by swinging the hands.

- The hip and knee joints do not move with significant force from an upright position in tap dancing. The activity of the biceps femoris and the gluteus maximus muscles are approximately 0.5, even at instantaneous maximum values, which is not high compared to other muscle activity.

- Motion of the ankle joint plays an important role in tap dancing. This can be inferred from the remarkable activity of the tibialis anterior and gastrocnemius.

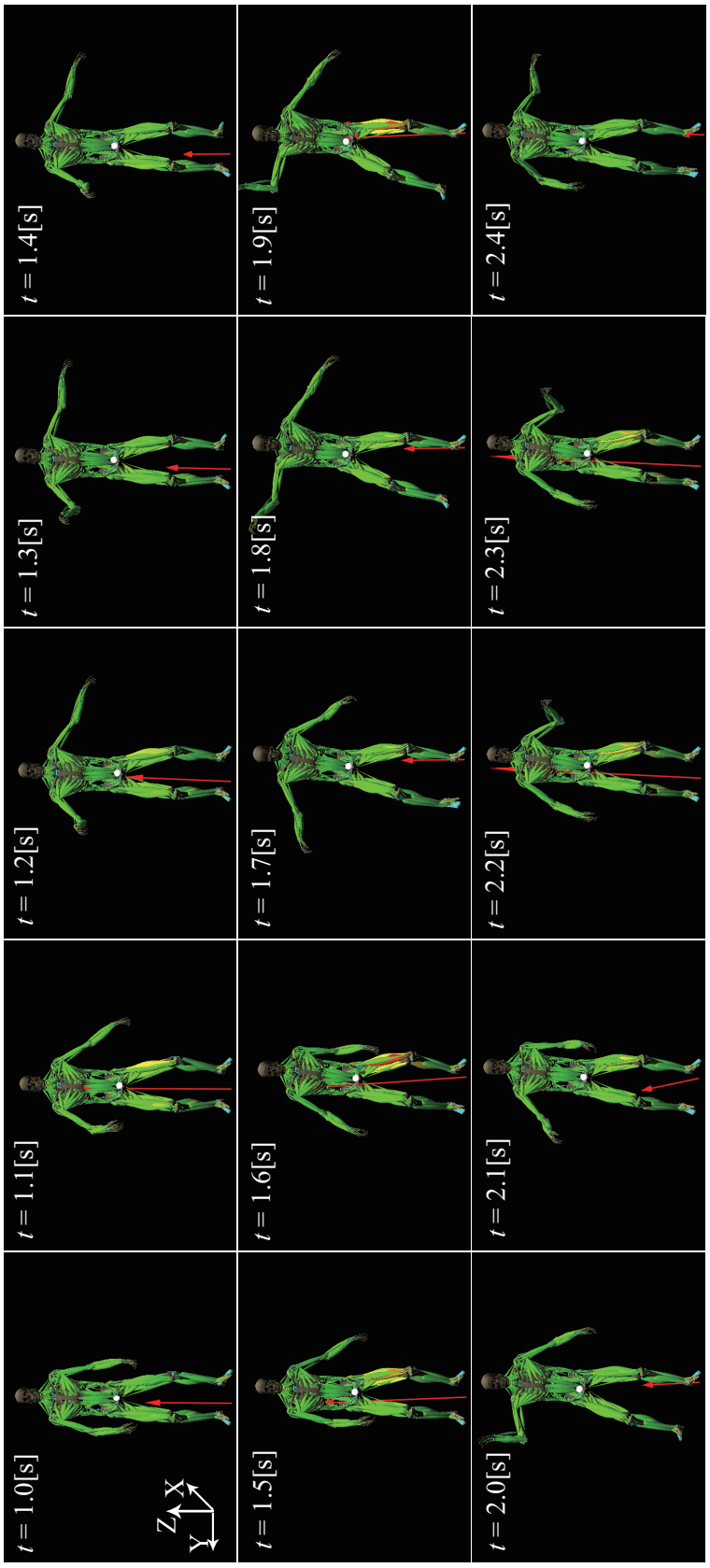

Figure 5.4: Snapshots of the Tap Dance motion

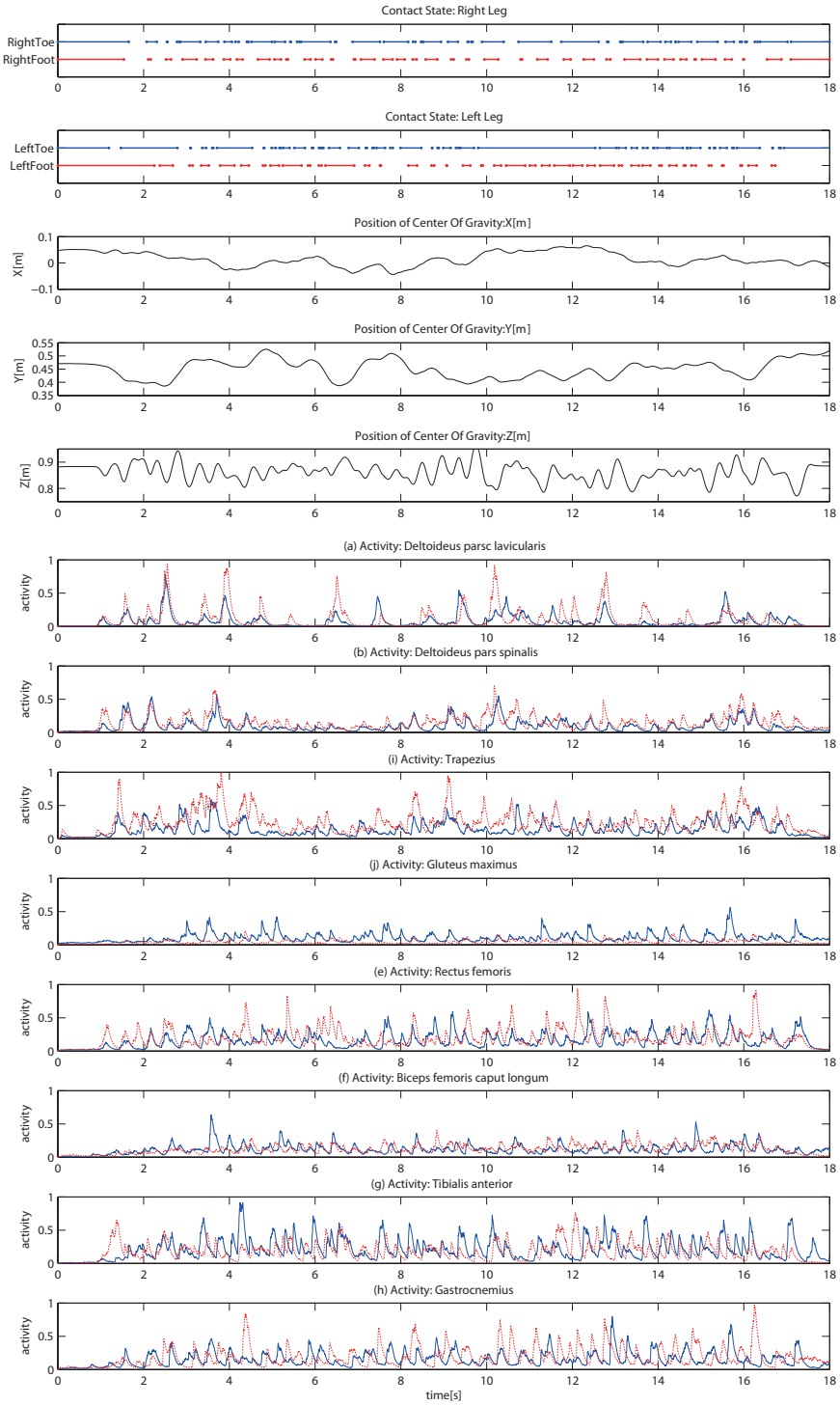

Figure 5.5: Tap Dance motion: Contact state (dots mean touch or leave events and line shows the "touch" state), position of COG and activation of major 16 muscles (Blue line shows the right side of the body, red dot shows left side of the body)

5.3.3 Drum playing

Based on a skilled drummer, ideal motion during playing involves the stable condition of the trunk. There is no awareness that the player is using muscles, and fatigue is not easily encountered during long playing periods. Twenty seconds of playing were analyzed with three drums (snare drum, high tom, and low tom). Contact force on the snare head and timing of the attack were calculated from the acceleration of the stick and the timing of the sound. Figure 5.6 shows snapshots of drum playing. Figure 5.7 shows the score, height of the COG, and 16 major muscle activities. For convenience, the motion was separated into four phases:

- Phase 1: (12–17.5 s) Hi-hat, snare drum, bass drum
- Phase 2: (17.5–21 s) Ride cymbal, snare drum, bass drum
- Phase 3: (21–27 s) Crush cymbal, ride cymbal, snare drum, and bass drum
- Phase 4: (27–29 s) Snare drum, hi-tom and low-tom

The crash cymbal, ride cymbal, and hi-hat are played by the right hand, the bass drum by the right foot, the snare drum by the left hand, and the hi- and low-toms by both hands. Measured muscles were changed partially to the (k) brachioradialis and (l) external oblique muscles. The following considerations are based on the analysis results.

- The COG did not change significantly. The average COG height over 10–12 s in the Z direction in the initial static posture was 0.4458 m, while that over 12–30 s during exercise was 0.4453 m (with a variance of 7×10^{-6} m ^{2}).

  Figure 5.7 shows the change of the COG in the XY plane (10–30 s). The position of the COG was different for each phase. The reason for the large COG swing over 30 s was the drummer 's attempt to mute the cymbal, and not because of the playing itself. Except for that maneuver, the COG moved 40 mm and 15 mm in the X- and Y-axes at most, which is a small amount.

- Muscle activity depends on the specific musical instrument. Radial arm muscle activity was particularly noticeable: for the hi-hat, the right radial muscle was

prominent; for the bass drum, the right gastrocnemius; for the ride cymbal, the right radial muscle and right anterior deltoid; for the crash cymbal, the right radial muscle, anterior deltoid, and biceps; for the snare drum, the right and left radial muscles, right rear deltoid, and left biceps; and for the tom-tom, the right and left radial muscles, left biceps, and right rear deltoid.

In particular, significant activity changes of the right deltoid muscle were observed in each phase. This is attributed to changes in the movement from the Z-axis direction to the X-axis direction during changes from Phase 1 to Phase 2. In addition, the triceps and biceps worked remarkably well with respect to Phases 3 to 4. Because of the arm position close to the body trunk in phase 4, the rear deltoid muscle worked significantly.

- Z-axis movement of the COG correlated with the performance of the bass drum by the right foot and the snare drum by the left hand. This is because the motion of the two above-mentioned behaviors is most striking in the vertical direction. On the other hand, playing cymbals in the right hand influenced the motion of the COG toward the X and Y directions.

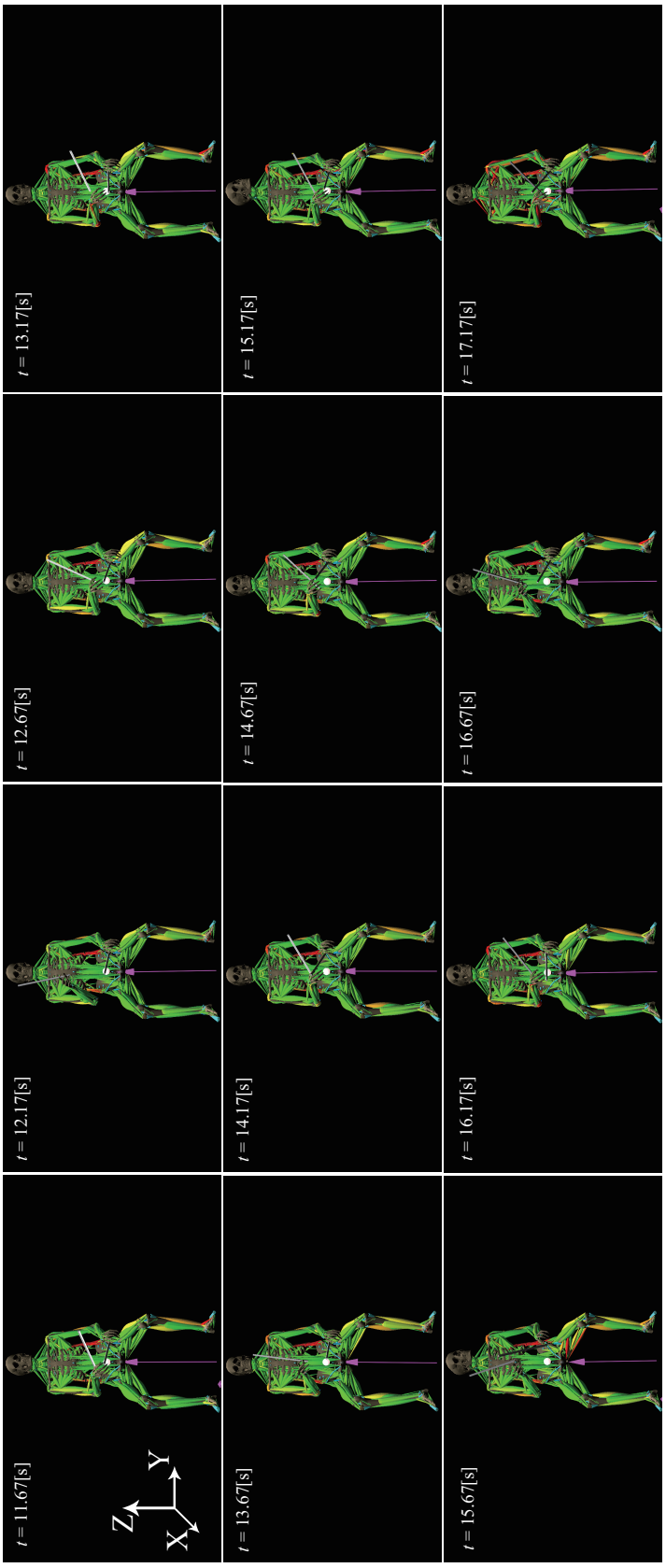

Figure 5.6: Snapshots of the drum playing.

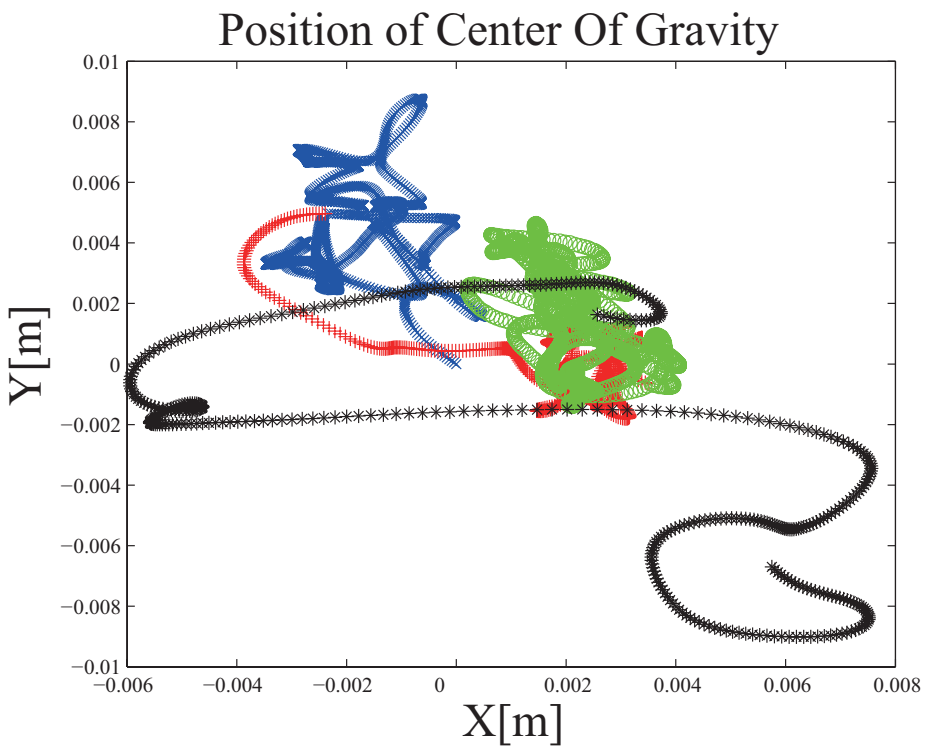

Figure 5.7: Position of the COG in the XY plane; the origin was set at 12 s.

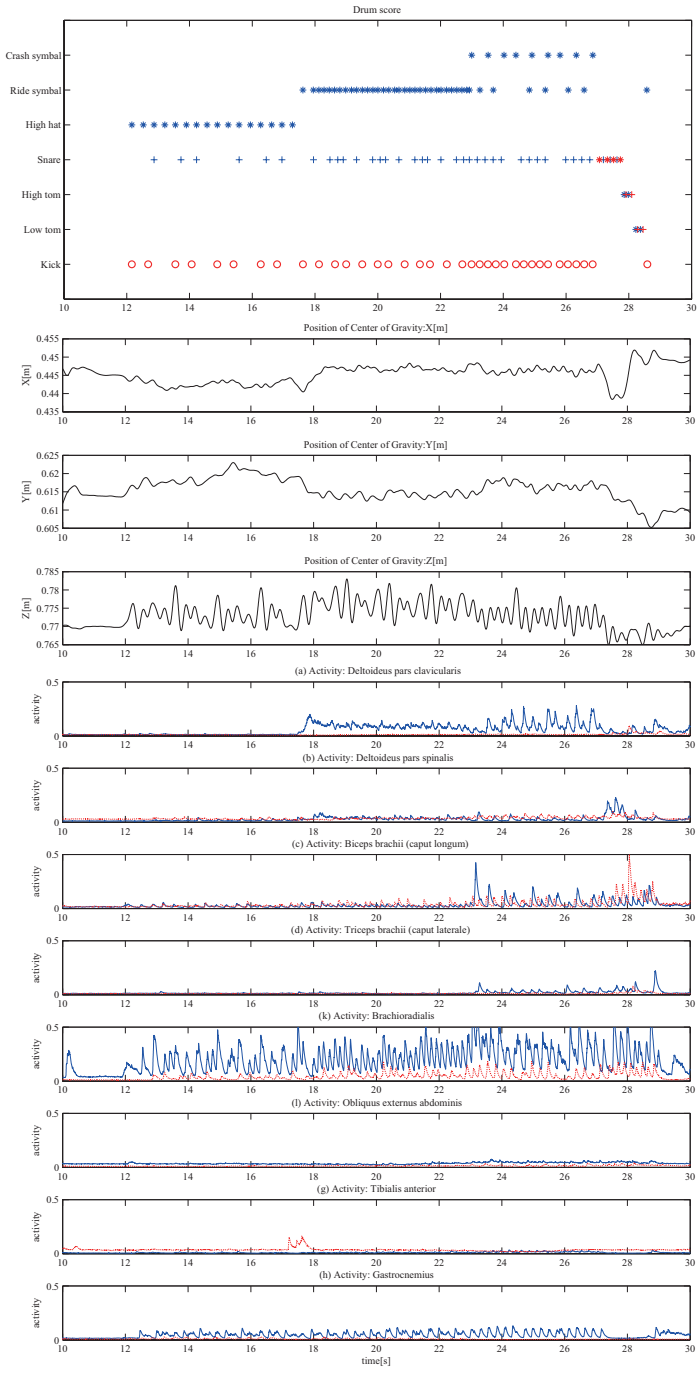

Figure 5.8: Drum playing: Contact state, position of COG and Activation of major 16 muscles. The motion is divided into 4 motion phase, Phase(1) 12-17.5[s], Phase (2) 17.5-21[s], Phase (3) 21-27[s] and Phase (4) 27-29[s].Score: * shows the timing of right hand contact, + shows left hand contact, o shows right foot contact. Muscle activation: Blue line shows the right side of the body, Red dot shows left side of the body.

The following sections are to be appeared in the publication (in preparation).

Chapter6

Musculoskeletal Morphing Between Different Species of Mammals, from Human to Mouse

6.1 Introduction

In this chapter, modeling of the musculoskeletal system of an experimental mouse is presented. As discussed in the previous chapter, experimental mice are widely used in the fields of biology and medicine. In a study of genetic diseases, the research findings obtained from mouse experiments are employed in the medical field for humans. However, most genetic studies have focused on the cell phenotype or social behaviors, and studies of the motor functions, which are the joint torques or muscle tensions, are rare. For advanced study of the motor functions of experimental mice, a musculoskeletal model is required.

Although some of the literature has discussed the skeletal system of a mouse [10], there are not many works on the modeling of the musculotendinous system of a mouse or even other mammals. As done for humans, MRI and CT imaging is the main source of anatomical information. Since the resolution of MRI imaging depends on the relative scales of the animals and excitation coils, technical difficulties exist for small animals. X-ray CT scanning is the most useful for small laboratory animals owing to the fact that the problem of radiation exposure is not too critical for these animals. The ANR project has conducted a musculoskeletal analysis for a laboratory rat based on the X-ray CT scanning [27]. More recently, Oota et al. [36, 37] developed a model of the skeletal system of a laboratory mouse based on X-ray CT scanning;

however, modeling of the entire musculotendinous system is still a future problem.

On the other hand, there are many publications on the modeling and analysis of the human musculoskeletal system based on the rich accumulation of anatomical and physiological knowledge [12, 24]. Nakamura et al. developed a whole-body model of the human musculoskeletal system that is appropriate and consistent with algorithms for robotic kinematic and dynamic computation [31, 32, 34] and proposed an optimization algorithm to estimate muscle activities on the basis of the information obtained by a motion capture system and other sensory systems. The developed software and measurement system have been applied to the analysis of human motions.

This chapter describes a systematic method for building a musculotendinous model of a mammal—specifically, a laboratory mouse. The use of MRI/CT imaging is assumed for fine anatomical agreement. However, our main proposal is the use of a human musculotendinous model, which is precisely developed and transferred to build a preliminary model for another mammal before fine anatomical adjustments using the MRI/CT image data. This approach relies on the homology between mammalian species. The proposed method consists of two consecutive steps. The first step is to find a geometrical morphing map from one bone of the human skeletal system to the corresponding bone of another mammalian species—namely, a laboratory mouse. The second step uses the geometrical morphing maps of bones to transfer the terminal and via points of the elements of the human musculotendinous system to those of the mouse musculotendinous system. Moreover, this chapter presents the results of a muscle length analysis from the motion capture data of a mutant nude mouse.

The following sections are to be appeared in the publication (in preparation).

Chapter7

Muscle Force Estimation for the Behavioral Analysis of Mutant Mice

7.1 Introduction

Along with the developments in genetic modification technology, the significance of mouse-motion measurement and its analysis have increased. It is necessary to quantitatively evaluate the motion of mice, particularly in forward genetics, which introduces random mutations. Devices for the assessment of the motion function, such as the rotor rod, treadmill, and the grip strength measuring device, are used in screening experiments. The rotor rod measures the time during which there is no fall from the rotating cylinder, the treadmill measures the distance and the number of times that an electric shock is given, and the strength measuring device measures the maximum force of the cling grip. A simple device is required to accomplish the numerous screening tests. In these devices, the number of evaluable functions are limited. Therefore, they are not suitable for high-dimensional testing. There is a ladder for observing the mouse walking pattern [22, 41]. The time for each walking step and the number of stepping failures can be measured. Although this ladder can be used for measuring the learning functions, it cannot be used for the analysis of the gait motion.

Pearson et al. [38, 4] developed a needle electromyogram (EMG) device for mice and analyzed the walking motion, combined with camera images. They measured the walking motion of mutant mice (Wph-4) and controlled mice, and reported the vastus

latetalis usage characteristics. Considering rats, which are also model animals slightly larger than mice, the walking motion was analyzed using X-ray images. Mice-bone motion measurements have been performed by ANR projects [27]. However, none of these studies treat the dynamics of the body mass and the use of muscle tension or torque has not been reported thus far.

Powerful tools have been developed in the field of robotics for the estimation of the force dimension by the non-invasive observation of motion [32]. If we can simulate the measured mouse motion in a computer and obtain the estimated joint torques or the tension of each muscle, non-invasive testing is possible for natural motion analysis. We can test the motor skill acquisition process, owing to the environment and assess the changes.

As mice have small mass, the resultant error from the dynamics simulator becomes relatively large. The assessment of the contact reaction force, during motion measurement, is necessary for a better torque estimation calculation. The use of a reaction force sensor is a good option because it can be non-invasively incorporated into the experimental system. We have developed a force measurable ladder for experimental mice and have estimated their inertial parameters. Motion analysis in the force dimension is performed through the measurement of the walking motion of mutant mice and reported in this chapter.

The following sections are to be appeared in the publication (in preparation).

Chapter8

Conclusion

This dissertation studies the subject-specific modeling of bodies and the modeling of contacts with environment, which are required for the estimation of muscle forces from noninvasive measurement data on the basis of geometric characteristics for the individuals'.

Important findings obtained in this dissertation are summarized as follows:

(1) The fundamental and simple-manner techniques of muscle modeling and inertial parameter modeling for large-DOF musculoskeletal systems on the basis of geometric characteristics of bodies were developed. Not only for the humans, but also through the modeling of heterogeneous mammals, especially for the mice, the wide range of applicability of developed techniques was perceived.

(2) Through the development of the contact modeling, the method of practical motion analysis combined with multiple people was proposed. Especially, practical contact force estimation in multipoint became possible by solving the optimization problem for contact forces and muscle forces simultaneously considering force directions and somatosensory electromyography signals even if the contact forces could not be measured directly.

(3) The quantitative assessment techniques for the large-DOF whole-body motor functions of the laboratory mice was newly developed ahead of the world through the presentation of the measurement techniques and the analysis results, which include the time-series data of the muscle tensions, joint torques, and joint trajectories.

The results obtained from the work presented in this dissertation are to be appeared in the publication (in preparation).

The detail of the features and the methods, their results, and the conclusions of each chapter are summarized as follows:

In Chapter 3, the identification of the geometric and inertial parameters for a subject-specific model using body-geometry polygonal models was presented. There existed a method for identifying the kinematic or inertial parameters of lower–degrees-of-freedom (DOF) human figures up to 15 segments, did not for the larger-DOF musculoskeletal system. For extending the lower-DOF model, an identification process that uses a time series of the motion data was presented. As an attempt to increase the estimation accuracy of the inertial parameters, the parameters were calculated beforehand on the basis of a geometric polygonal model found in database. Subject-specific kinematic parameters were identified by solving for the introduced inverse-kinematic time-invariant variables, which was the link length. The base parameter of the kinematically identified model for each link was obtained by a sequential identification method [7, 45, 5, 47, 46, 6]. The subject-specific inertial data could be estimated by the sum of the mass points arranged at regular intervals inside the body shape obtained from database. Furthermore, a weight map function obtained from the distances between distributed mass points and body links was introduced. Using the weight map proposed in Chapter 2, the deviation in the mass parameters for the spine links could be reduced. The inertial parameters were calculated using a quadratic programming method satisfying the conditions of the base and inertial parameters obtained previously. The obtained results were all of the inertial parameters that satisfy the physical consistency of the parameters. The experimentally measured data related to the force acting on the base link and the force calculated from the identified inertial model were compared to validate the identified model. The proposed method could provide simple subject identification method since the required reference motion data were one.

In Chapter 5, the dynamics simulation results based on the method presented in Chapter 4 using the identified subject-specific model based on the method presented

in Chapter 3 were analyzed. Chapter 5 also presented the results of an analysis of experts' motions using the generated individual musculoskeletal model described in Chapter 4. For the calculation, the method introduced and proposed in Chapter 4 is applied to each case. We covered elite athletes' motions that had not quantified and visualized so far (Tai Chi, tap dance, drum performance, and Judo). Methods for measuring the somatosensory signals by EMG and the floor reaction forces as well as the motion capture system were described. The data for the COG, joint angle, contact force, muscle activity, and muscle tension were analyzed, and the characteristics of the data were described. By understanding the actions of elite players, a greater understanding of the motions for these techniques could be obtained.

Bibliography

[1] Mouse genom informatics. http://www.informatics.jax.org/. Accessed: 2010.

[2] Blasdel Aaron, Yosuke Ikegami, Ko Ayusawa, and Yoshihiko Nakamura. Balancing anatomy and function in a musculoskeletal model of hands. *Proc. of the IEEE Int. Conf. on Robotics and Automation*, 2012.

[3] Michiyoshi Ae, Hai peng Tang, and Takashi Yokoi. Estimation of inertia properties of the body segments in japanese athletes. *Journal of the Society of Biomechanisms Japan*, 11:23–33, 1992-05-20 (in Japanese).

[4] T Akai, H J Acharya, K Fouad, and K G Pearson. Behavioral and electromyographic characterization of mice lacking epha4 receptors. *J Neurophysiol*, 96:642–651, 2006.

[5] K. Ayusawa, G. Venture, and Y. Nakamura. Identification of humanoid robots dynamics using floating-base motion dynamics. *Proc. of IEEE/RSJ International Conference on Intelligent Robots and Systems*, pages 2854–2859, 2008.

[6] K. Ayusawa, G. Venture, and Y. Nakamura. Symbolic proof of inertia-parameter identifiability of legged mechanisms from unactuated base-link dynamics. *Proc. of 15th IFAC Symposium on Systems Identification*, pages 693–698, 2009.

[7] K. Ayusawa, G. Venture, and Y. Nakamura. Real-time implementation of physically consistent identification of human body segments. *Proc. of the IEEE Int. Conf. on Robotics and Automation*, pages 6282–6287, 2011.

[8] Ko Ayusawa and Yoshihiko Nakamura. Fast inverse dynamics algorithm with decomposed computation of gradient for wire-driven multi-body systems and its application to estimation of human muscle tensions. *2nd IFToMM International Symposium on Robotics and Mechatronics*, (11), 2011.

[9] Ko Ayusawa and Yoshihiko Nakamura. Fast inverse kinematics algorithm for large dof system with decomposed computation of gradient and its application to musculoskeletal model. *17th Robotics Symposia (in Japanese)*, (2B4), 2011.

[10] Itai Bab, Carmit Hajbi-Yonissi, Yanken Gabet, and Ralph Muller. *Micro-Tomographic Atlas of the Mouse Skeleton*. Springer, 2007.

[11] Edward K. Chadwick, Dimitra Blana, Antonie J. van den Bogert, and Robert F. Kirsch. A real-time, 3d musculoskeletal model for dynamic simulation of arm movements. *IEEE Transactions on Biomedical Engineering*, 56(4):941–948, 2009.

[12] Carmine D Clemente. *Anatomy A Regional Atlas of the Human Body*. Lippincott Williams & Wilkins, 2007.

[13] Charles Darwin. *The Origin of Species*. London:John Murray, 1859.

[14] Richard Dawkins. *The Selfish Gene*. Oxford University Press, 1989.

[15] S.L. Delp and J.P. Loan. A graphics-based software system to develop and analyze models of musculoskeletal structures. *Computers in Biology and Medicine*, 25(1):21 – 34, 1995.

[16] S.L. Delp and J.P. Loan. A computational framework for simulating and analyzing human and animal movement. *IEEE Computing in Science and Engineering*, 2(5):46–55, 2000.

[17] E. Forster, U. Simon, P. Augat, and L. Claes. Extensionof a state-of-art optimization criterion to predict co-contraction. *Jornal of Biomechanics*, 37(4):577–581, 2004.

[18] Harold M Frost. *The Utah Paradigm of Skeletal Physiology*. 1960.

[19] Harold M Frost. Skeletal structural adaptations to mechanical usage (satmu): 1. redefining wolff's law: the bone modeling problem. *The Anatomical Record*, 4(226):403–413, 1990.

[20] Harold M Frost. Defining osteopenias and osteoporoses: Another view (with insights from a new paradigm). *Bone*, 20(5):385–391, 1997.

[21] Harold M Frost. The utah paradigm of skeletal physiology: an overview of its insights for bone, cartilage and collagenous tissue organs. *J. Bone Miner Metab*, 18:305–316, 2000.

[22] Ruben S. Van Der Giessen, Sebastiaan K. Koekkoek, Stijn van Dorp, Jornt R. De Gruijl, Alexander Cupido, Sara Khosrovani, Bjorn Dortland, Kerstin Wellershaus, Joachim Degen, Jim Deuchars, Elke C. Fuchs, Hannah Monyer, Klaus Willecke, Marcel T.G. De Jeu, and Chris I. De Zeeuw. Role of olivary electrical coupling in cerebellar motor learning. *Neuron*, 58(4):599 – 612, 2008.

[23] J W Gordon, G A Scangos, D J Plotkin, and et al. Genetic transformation of mouse embryos by microinjection of purified dna. *Proc. of National Academy of Sciences of the United States of America*, 77(12):7380–7384, 1980.

[24] Sho Itoh and Yasuyoshi Yokokohji. Function analysis of intrinsic muscles of human hand based on musculo-skeletal model. *The 28th Annual Conference of the Robotics Society of Japan (Japanese)*, page AC2O2, 2010.

[25] Adam G. Kirk, James F. O'Brien, and David A. Forsyth. Skeletal parameter estimation from optical motion capture data. In *IEEE Conf. on Computer Vision and Pattern Recognition (CVPR) 2005*, pages 782–788, June 2005.

[26] Ko Ayusawa and Yosuke Ikegami and Yoshihiko Nakamura. Simultaneous Geometric Parameters Identification and Inverse Kinematics of Time Series Motion by Fast Optimization Using Decomposed Gradient Computation. *Proc. of the Conf. on Robotics and Mechatronics*, pages 2P1–O10, 2012 (in Japanese).

[27] T Lelarda, M Jamonc, J P Gascb, and P P Vidal. Postural development in rats. *Experimental Neurology*, 202(1):112–124, 2006.

[28] H. Mayeda, K. Osuka, and A. Kanagawa. A new identification method for serial manipulator arms. In *Proc. of 9th IFAC World Congress*, volume 2, pages 74–79, 1984.

[29] M. Mochimaru and M. Kouchi. Japanese body dimension data. *http://riodb.ibase.aist.go.jp/dhbodydb/97-98/index.html.en*, 1997-98.

[30] Akihiko Murai, Kosuke Kurosaki, Katsu Yamane, and Yoshihiko Nakamura. Musculoskeletal-see-through mirror: Computational modeling and algorithm for whole-body muscle activity visualization in real time. *Biophysics and Molecular Biology*, 3(103):310–317, 2010.

[31] Y Nakamura, K Yamane, I Suzuki, and Y Fujita. Dynamic computation of mucsculo-skeletal human model based on efficient algorithm for closed kinematic chains. *Proc. of the 2nd International Symposium on Adaptive Motion Animals and Machines*, pages SaP–I–2, 2003.

[32] Y Nakamura, K Yamane, I Suzuki, and Y Fujita. Somatosensory computation for man-machine interface from motion capture data and musculoskeletal human model. *IEEE Transactions on Robotics*, 2005.

[33] Yoshihiko Nakamura and Katsu Yamane. Dynamics computation of structure-varying kinematic chains and its application on human figures. *IEEE Transaction on Robotics and Automation*, 2000.

[34] Yoshihiko Nakamura, Katsu Yamane, and Akihiko Murai. Macroscopic modeling and identification of the human neuromuscular network. *Annual International Conference of the IEEE Engineering in Medicine and Biology Society*, pages 99–105, 2006.

[35] National Institute of Bioscience and Human-Technology, editors. *Japanese Body Dimension Data for Ergonomic Design*. Nippon Shuppan Service, 1996.

[36] S Oota, K Mekada, Y Fujita, J Humphpheries, K Fukami-Kobayashi, Y Obata, T Rowe, and A Yoshiki. Four-dimensional quantitative analysis of the gait of mutant mice using coarse-grained motion capture. *Proc. of IEEE Engineering in Medicine and Biology Society*, pages 5227–5230, 2009.

[37] S Oota, A Yoshiki, Y Fujita, J Humpheries, K Fukami-Kobayashi, Y Obata, T Rowe, and Y Nakamura. Development of a coase-grained skeletal model of laboratory mouse and its application. *Proc. of 1st Int'l Conf. on Applied Bionics and Biomechanics*, 2010.

[38] K G Pearson, H Acharya, and K Fouad. A new electrode configuration for recording electromyographic activity in behaving mice. *J. Neuroscience Methods*, 148:36–42, 2005.

[39] J. Rasmussen, M. Damsgaard, and M. Voigt. Muscle recruitment by the min/max criterion - a comparative numerical study. *Jornal of Biomechanics*, 34(3):409–415, 2001.

[40] H Roesler. Some historical remarks on the theory of cancellous bone structure (wolff's law). *Mechanical Properties of Bone*, 15:27–42, 1981.

[41] Estelle Rousselet, Chantal Joubert, Jacques Callebert, Karine Parain, Leon Tremblay, Gael Orieux, Jean-Marie Launay, Charles Cohen-Salmon, and Etienne C Hirsch. Behavioral changes are not directly related to striatal monoamine levels, number of nigral neurons, or dose of parkinsonian toxin mptp in mice. *Neurobiology of Disease*, 14(2):218 – 228, 2003.

[42] Ajay Seth, Michael A Sherman, Jeffrey A Reinboltb, and Scott L Delp. Opensim: a musculoskeletal modeling and simulation framework for in silico investigations and exchange. *Procedia IUTAM*, 2:212–232, 2011.

[43] Michael A Sherman, Ajay Seth, and Scott L Delp. Simbody: multibody dynamics for biomedical research. *Procedia IUTAM*, 2:241–261, 2011.

[44] R.H. Tamarin. *Principles of genetics*. WCB/McGraw-Hill, 1999.

[45] G. Venture, K. Ayusawa, and Y. Nakamura. Human and humanoid identification from base-link dynamics. *Proc. of IEEE RAS/EMBS International Conference on Biomedical Robotics and Biomechatronics*, pages 445–450, 2008.

[46] G. Venture, K. Ayusawa, and Y. Nakamura. Identification of human mass properties from motion. *Proc. of 15th IFAC Symposium on Systems Identification*, pages 988–993, 2009.

[47] G. Venture, K. Ayusawa, and Y. Nakamura. Real-time identification and visualization of human segment parameters. *Proc. of IEEE EMBS Annual International Conference*, pages 3983–3986, 2009.

[48] R H Waterson and et al. Initial sequencing and comparative analysis of the mouse genome. *Nature*, 420(6915):520–562, 2002.

List of Publications

Reviewed Conference Proceedings

[1] Akihiro Yoshimatsu, Yousuke Ikegami, Ko Ayusawa and Yoshihiko Nakamura, "Morphing Skeleton Model from Human to Mouse Based on The Links of Bones." Proc. of the 18th Robotics Symposia, Yamagata, Japan, 2013 (in Japanese).

[2] Yosuke Ikegami, Ayusawa Ko and Yoshihiko Nakamura, "Identification of Kinematic and Inertial Parameters for Subject-specific Human Musculoskeletal Model with Body Shape Information." Proc. of the 2nd IFToMM ASIAN Conference on Mechanism and Machine Science, Tokyo, Japan, 2012.

[3] Ko Ayusawa, Yosuke Ikegami and Yoshihiko Nakamura, "Simultaneous Solver for Kinematic Identification and Inverse Kinematics of Human Skeletal Model from Motion Capture Data." Proc. of the 2nd IFToMM ASIAN Conference on Mechanism and Machine Science, Tokyo, Japan, 2012.

[4] Yosuke Ikegami, Ayusawa Ko and Yoshihiko Nakamura, "Masters' Skill Explained by Visualization of Whole-Body Muscle Activity." Proc. of the 3rd International Conference on Simulation, Modeling, and Programming for Autonomous Robots, Tsukuba, Japan, 2012.

[5] Blasdel Aaron, Yosuke Ikegami, Ayusawa Ko and Yoshihiko Nakamura, "Balancing Anatomy and Function in a Musculoskeletal Model of Hands." Proc. of the 2012 IEEE Int. Conf. on Robotics and Automation, St. Paul, United States, 2012.

[6] Yoshihiko Nakamura, Yosuke Ikegami, Akihiro Yoshimatsu, Ko Ayusawa, Hirotaka Imagawa, Satoshi Oota. "Musculoskeletal morphing from human to mouse. " Proc. of the IUTAM Symposium on Human Body Dynamics, Waterloo, Canada, 2011.

Oral Presentations

[1] Takanori Ishii, Yoshihiko Nakamura, Yosuke Ikegami, Naoki Itami and Seiji Miyazaki, "Kinematic Characteristics of Elite Judo Athelete in Uchimata Motion." 5th National Strength and Conditioning Association International Conference, OJ-08 303, Chiba, Japan, 2017 (in Japanese).

[2] Ayaka Yamada, Yosuke Ikegami and Yoshihiko Nakamura, "Research of Sports Training Based on Biomechanics: Analysis of Estimated Muscle Tension Forces about Double Leg Circles on Pommel Horse." The 17th SICE System Integration Division Annual Conference, 2O1-1, Hokkaido, Japan, 2016 (in Japanese).

[3] Motoyuki Nawa, Kazuie Nishiwaki, Kyoji Yamawaki, Yosuke Ikegami, Ayaka Yamada, Yohan Shin and Yoshihiko Nakamura, "Comparison of Performance of Circles and Their Relevant Techniques on a Pommel Horse, and Its Evaluation Method." Proc of the JSME Symposium: Sports and Human Dynamnics 2016, No.16-40, Yamagata, 2016 (in Japanese).

[4] Jose Enrique Chen, Yosuke Ikegami, Motoyuki Nawa, Kazuie Nishiwaki, Kyoji Yamawaki and Yoshihiko Nakamura, "Centroidal Dynamics of a Double Leg Circle Motion on a Pommel Horse." The 34th Annual Conference of the Robotics Society of Japan, 3W3-08, Yamagata, 2016.

[5] Motoyuki Nawa, Kazuie Nishiwaki, Kyoji Yamawaki, Yosuke Ikegami, Yoshihiko Nakamura, Akihiko Murai, Ko Ayusawa and Taiga Yamasaki, "An Evaluation of Performance of a Double-Leg Circle on a Pommel Horse, and a Desirable Performance Proposal." International society of biomechanics in sports, Tsukuba, Japan, 2016.

[6] Yosuke Ikegami, Rohan Budhiraja, Ayaka Yamada, Akio Hayakawa and Yoshihiko Nakamura, "Neuromusculoskeletal Simulator: On Spinal Neural Networks and Body Parameters." International Workshop on Supercomputational Life Science 2015, Tokyo, Japan, 2015.

[7] Motoyuki Nawa, Kazuie Nishiwaki, Kyoji Yamawaki, Yosuke Ikegami, Yoshihiko Nakamura, Akihiko Murai, Ko Ayusawa and Taiga Yamasaki, "The Mechanism of a Double-Leg Circle on a Pommel Horse, and Its Variation of Performance." Proc of the JSME Symposium: Sports and Human Dynamnics 2015, C-3, Yamagata, 2015 (in Japanese).

[8] Kazunari Takeichi, Akihiko Murai, Yosuke Ikegami and Yoshihiko Nakamura, "Total synthesis of FEM musculoskeletal system and spiking neural networks in the spinal cord." Workshop on HPCI Strategic Program Field 1, Hyogo, 2015 (in Japanese).

[9] Yosuke Ikegami, Ko Ayusawa and Yoshihiko Nakamura, "Simultaneous kinematic and inertial parameter identification method for subject-specific human musculoskeletal model using body shape information." Proc. of the 30th annual conference of the robotics society of japan, 2012, Hokkaido, Japan, 2012 (in Japanese).

[10] Yoshimatsu Akihiro, Yosuke Ikegami, Ko Ayusawa and Yoshihiko Nakamura, "Construction of Individual Human Whole Body Model through Musculoskeltal Morphing." Proc. of the 29th annual conference of the robotics society of japan, 2012, Hokkaido, Japan, 2012 (in Japanese).

[11] Yosuke Ikegami, Ko Ayusawa and Yoshihiko Nakamura, "Identification of subject-specific geometric and inertial parameters for human musculoskeletal model." Proc. of 2012 JSME Conference on Robotics and Mechatronics, 2P1-O11, 2012 (in Japanese).

[12] Ko Ayusawa, Yosuke Ikegami and Yoshihiko Nakamura, "Simultaneous geometric parameters identication and inverse kinematics of time series motion by fast optimization using decomposed gradient computation." Proc. of 2012 JSME Conference on Robotics and Mechatronics, 2P1-O10, 2012 (in Japanese).

[13] Sreenivasa Manish, K. Mombaur, P. Soueres, Yosuke Ikegami, Yoshihiko Nakamura, "Optimal control in the manipulation of complex objects: human yo-yo playing." 9th Winter workshop on Mechanism of Brain and Mind, Hokkaido, 2012.

[14] Yosuke Ikegami, Ko Ayusawa, Taku Kashiwagi, Kanade Kubota, Akihiro Yoshimatsu, Yusuke Nakamura, Yuki Ibuka, Jun'ichi Ishikawa, Shun-Chieh Hung, ChangHeon Yi, Aaron Blasdel, Yoshihiko Nakamura, "Visualization of experts ' motion skill based on the whole body muscle tension estimation." Proc of the JSME Symposium: Sports and Human Dynamnics 2011, Kyoto, Japan, 2011 (in Japanese).

[15] Motoyuki Nawa, Kazuie Nishiwaki, Yoshihiko Nakamura, Yosuke Ikegami, Ko Ayusawa, Kiyoshi Goto, Daisuke Goto, "An analysis of the motion in a side horse exercise. " Proc of the JSME Symposium: Sports and Human Dynamics 2011, kyoto, Japan, 2011 (in Japanese).

[16] Satoshi Oota, Yosuke Ikegami, Ko Ayusawa, Kazuyuki Mekada, Nobunari Kakusho, Hirotaka Imagawa, Hiroyuki Hishida, Hiromasa Suzuki, Yuichi Obata, Hideo Yokota, Ryutaro Himeno, Yoshihiko Nakamura, Atsushi Yoshiki, "Towards fine-grained phenotypic analyses of motor functions: the inverse kinematics of mouse gait patterns. " Proc. of the 25th International Mammalian Genome Society, Mouse Genetics 2011, Washington DC, USA, 2011.

[17] Satoshi Oota, Yosuke Ikegami, Ko Ayusawa, Nobunari Kakusho, , Hiroyuki Hishida, Hiromasa Suzuki, Yuichi Obata, Ryutaro Himeno, Yoshihiko Nakamura, Atsushi Yoshiki, "Fine-grained phenotypic analyses of motor functions for laboratory mice : the inverse kinematics of mouse gait patterns. " The 34th Annual Meeting of the Japan Neuroscience Society, vol. 71, sup. 1, pp. 244, 2011.

[18] Yosuke Ikegami, Akihiro Yoshimatsu, Ko Ayusawa, Satoshi Oota, Yoshihiko Nakamura, "Musculoskeletal morphing from human to mouse and muscle tension analysis. " The 49th Annual Meeting of the Biophysical Society of Japan, 2011.

[19] Yosuke Ikegami, Ko Ayusawa, Yoshihiko Nakamura, "High Performance Computing of Neuro Biomechanics." The Symposium on Super Computing 2010, Kobe, Japan, 2010 (in Japanese).

[20] Satoshi Oota, Nobunori Kakusho, Yosuke Ikegami, Kazuyuki Mekada, Koh Ayusawa, Hirotaka Imagawa, Yuichi Obata, Ryutaro Himeno, Hideo Yokota, Yoshihiko Nakamura, and Atsushi Yoshiki, "Homology mapping: development of the mouse hindlimb musculoskeletal model using the human musculoskeletal model and Scleraxis (Scx)-GFP mouse." Proc of the 24th International Mammalian Genome Conference (IMGC), Crete, Greece, 2010, October 17-20.